Available online at www.sciencedirect.com
SCIENCE DIRECT®
Biochemical and Biophysical Research Communications 336 (2005) 118–127
BBRC
www.elsevier.com/locate/ybbrc

Sonoporation using microbubble BR14 promotes pDNA/siRNA transduction to murine heart

Sei Tsunoda [a,b,c], Osam Mazda [c,*], Yohei Oda [a,b], Yasunori Iida [a,b,c], Satoshi Akabame [a,b], Tsunao Kishida [c], Masaharu Shin-Ya [c], Hidetsugu Asada [c], Satoshi Gojo [d], Jiro Imanishi [c], Hiroaki Matsubara [a], Toshikazu Yoshikawa [b]

[a] *Department of Molecular Cardiology and Vascular Regenerative Medicine, Graduate School of Medical Science, Kyoto Prefectural University of Medicine, Kyoto 602-8566, Japan*
[b] *Department of Inflammation and Immunology, Graduate School of Medical Science, Kyoto Prefectural University of Medicine, Kyoto 602-8566, Japan*
[c] *Department of Microbiology, Graduate School of Medical Science, Kyoto Prefectural University of Medicine, Kyoto 602-8566, Japan*
[d] *Department of Cardiovascular Surgery, Saitama Medical Center, Kawagoe, Saitama 350-8550, Japan*

Received 28 July 2005
Available online 18 August 2005

Abstract

Naked plasmid DNA (pDNA) and short interfering RNA (siRNA) duplexes were transduced into adult murine heart by means of sonoporation using the third-generation microbubble, BR14. Plasmid DNAs carrying luciferase, β-galactosidase (β-gal), or enhanced green fluorescent protein (EGFP) reporter genes were mixed with BR14 and injected percutaneously into the left ventricular (LV) cavity of C57BL/6 mice while exposed to transthoracic ultrasound at 1 MHz for 60 s. Sonoporation at an output intensity of 2.0 W/cm^2 and a 50% pulse duty ratio resulted in the highest luciferase expression in the heart. Histological examinations revealed significant expression of the β-gal and EGFP reporters in the subendocardial myocardium of LV. Intraventricular co-injection of siRNA-GFP and BR14 with concomitant ultrasonic exposure resulted in substantial reduction in EGFP expression in the coronary artery in EGFP transgenic mice. The present method may be applicable to gain-of-function and loss-of-function genetic engineering in vivo of adult murine heart.

Keywords: Naked plasmid DNA; Heart; Sonoporation; Microbubble; Gene transfer; RNA interference; Ultrasound; Gene therapy; Molecular therapy

Genetic modification of the heart may provide a powerful molecular tool for improving our understanding of cardiac diseases. Moreover, a technology that enables safe and efficient gene delivery to the heart may provide a novel therapeutic modality to control heart disorders. Some studies recently demonstrated that efficient transfer of genes into murine heart can be achieved by intracoronary infusion of adenoviral or adeno-associated viral vectors followed by transient aortic occlusion [1,2]. Viral vector-mediated procedures, however, may induce complications associated with recombinant viruses, hindering clinical application of the systems to gene therapy for cardiovascular diseases. Although non-viral methods are free from virus-associated adverse effects, their transduction efficiency is low. For example, following direct intramyocardial injection of plasmid DNA into the heart of mice [3], rats [4,5], and hamsters [6], the transgenes were expressed only within a small area surrounding the injection site.

* Corresponding author. Fax: +81 75 251 5331.
E-mail address: mazda@koto.kpu-m.ac.jp (O. Mazda).

0006-291X/$ - see front matter © 2005 Elsevier Inc. All rights reserved.
doi:10.1016/j.bbrc.2005.08.052

A more efficient non-viral method of gene transfer is sonoporation of cells. In sonoporation, ultrasound is used to increase the porosity of the cell membrane [7]. The ultrasound induces the formation of cavitation bubbles that by mechanical action cause enough damage to the cell membrane to allow large molecules in the surrounding medium to enter the cell, but not so much damage that the cell cannot reseal the membrane and survive [8]. The extent of cavitation bubble formation and subsequent increase in membrane permeability can be enhanced by use of microbubble echo contrast agents. This method has been applied to skeletal muscle of mice [9], as well as myocardium of both rats [10] and dogs [11], in vivo, using various microbubble agents including Levovist, Hexabrix, and Optison [9–18]. It has been indicated that the transfection efficiency is dependent on both the ultrasound parameters and the formulation of microbubbles.

BR14 (Bracco Research SA, Geneva, Switzerland) is a recently developed ultrasound contrast agent, which has some advantages over other echo contrast agents [19,20], because it consists of stabilized relatively small microbubbles and is transiently retained within capillaries. These qualities mean that BR14 may be a better agent in sonoporation-mediated transfection. Indeed, recent studies have indicated that BR14 effectively enhanced sonoporation-based gene transfection into hepatic cancer implant in mice [21] as well as into saphenous vein graft in porcine [22].

RNA interference (RNAi) is a powerful means of analyzing the function of genes in basic researches, while the technology may also be quite useful in developing therapeutic molecular targeting strategies for treatment of diseases. RNAi was first discovered in the nematode *Caenorhabditis elegans* as a response to double-stranded RNA, which induced sequence-specific silencing of gene expression [23]. In mammalian cells, short interfering RNA (siRNA) 21–23 nucleotide pairs in length silences the gene with the homologous sequence [23,24]. The in vivo effectiveness of siRNA-mediated silencing was also studied in various organs, including the liver [25,26] and the skeletal muscle [27]. However, in vivo RNAi in cardiac tissues has not been reported so far.

In the present study, we investigated whether BR14 facilitates sonoporation-mediated transfection of naked plasmid DNA into the adult murine heart. Moreover, we applied this method to transfer synthetic siRNA duplex, to knock down targeted genes in the heart in vivo.

Materials and methods

Animals. Female C57BL/6 mice (16.8 ± 0.7 weeks old, weighing 24.0 ± 0.5 g) were purchased from Shimizu Laboratory Suppliers (Kyoto, Japan). Enhanced green fluorescent protein (EGFP) transgenic mice (TGM) (27.3 ± 4.8 weeks old, weighing 25.3 ± 1.1 g) were purchased from Charles River Japan (Yokohama, Japan). All the animal experiments were performed according to the approved guidelines of Kyoto Prefectural University of Medicine.

Plasmid vectors and siRNA. The plasmids pGEG.GL3 [28], pGEG.EGFP [29], and pGEG.β [30] carried GL3 firefly luciferase (Luc), EGFP, and *Escherichia coli* β-galactosidase (β-gal) genes, respectively, under the control of the CAG promoter. Each plasmid also contained Epstein–Barr virus (EBV) nuclear antigen 1 (EBNA1) gene and EBV oriP sequence [31]. Plasmids were purified using Qiagen MegaPrep Endo-free kits (Qiagen, Hilden, Germany). siRNA duplex targeting GFP (siRNA-GFP) was purchased from Dharmacon (Lafayette, CO, USA).

In vivo experiments. Plasmid DNA (500 μg) or siRNA (40 μg) was diluted in 400 μl PBS and mixed with 100 μl BR14 microbubble. Mice were anesthetized by an intraperitoneal injection of sodium pentobarbital (40 μg/g body weight), and tracheotomy was performed in the supine position to provide ventilation via a ventilator (MiniVent 845; Hugo Sachs Elektronik, March-Hugstetten, Germany) at the rate of 150 cycles per min. An incision was made in the greater and smaller pectoral muscles, and the microbubble/nucleic acid solution was injected over a period of about 10 s into the left ventricular (LV) cavity via the intercostal muscle using a 27-gauge needle. The same solution was injected into the tail vein (TV) of another group of mice. At the same time as the initiation of the injection, transthoracic ultrasound insonation (sonication) was performed through a 6-mm diameter probe with an input frequency of 1 MHz, an output intensity of 1.0–2.0 W/cm^2, a pulse duty ratio (PDR) of 10–50%, and a duration of 60 s. A Sonitron 2000 (Rich-Mar, Inola, OK, USA) was used to generate the ultrasound. Hydrodynamics-based transduction was performed as described previously [28]. Briefly, 40 μg siRNA-GFP was diluted in 1600 μl PBS and injected intravenously within 4s via the tail vein using a 27-gauge needle.

Echocardiography and ECG monitoring. Transthoracic echocardiography was performed using an ultrasound platform (Nemio 30, Toshiba Medical, Tokyo, Japan) equipped with a 13-MHz imaging transducer. Under anesthesia, a parasternal view was obtained and M-mode images of the LV were recorded. Electrocardiographic monitoring was performed by limb lead (II) during the sonoporation.

Luciferase assay. Biventricular muscle was minced with a pair of scissors and homogenized in 200 μl of reporter lysis buffer (Promega, Madison, WI, USA) using a sonicator. The extract was centrifuged at 14,000*g* for 15 min, and the Luc activity in the supernatant was measured as described [32]. Organs other than the heart were also treated as described above. Protein concentration in the extract was determined as described previously [28].

X-gal staining. The heart was fixed with 4% paraformaldehyde and dehydrated in sucrose solution. The specimens were then stained with X-gal solution (0.05% (v/v) 5-bromo-4-chloro-3-indolyl-β-D-galactoside (X-gal; Nacalai Tesque, Kyoto, Japan), 1 mM $MgCl_2$, 150 mM NaCl, 3 mM $K_4[Fe(CN)_6]$, 3 mM $K_3[Fe(CN)_6]$, 60 mM Na_2HPO_4, 40 mM NaH_2PO_4, and 0.1% Triton X-100). After 12 h of incubation at 37 °C, the reaction was terminated by replacing the solution with PBS [33].

Fluorescence microscopic observation and immunohistochemistry. After perfusion with saline, the heart was fixed with 4% paraformaldehyde and dehydrated in sucrose solution. The specimens were embedded in OCT compound and immediately frozen at −80 °C. Serial sections 10 μm thick were cut on a cryostat and observed under a fluorescence microscope with excitation at 488 nm. The cryosections were stained with anti-GFP antibody (Molecular Probes, Leiden, The Netherlands) and visualized using the avidin/biotin/peroxidase method (Vector Laboratories, Burlingame, CA).

Statistical analysis. Differences among continuous variables were tested by Student's *t* test for paired and unpaired observations and by ANOVA with Fisher's PLSD correction for repeated comparisons. A value of $P < 0.05$ was considered to be statistically significant.

Results

Influence of sonoporation to the heart

A mixture of plasmid DNA and BR14 microbubble was injected into the LV of mice. Echocardiographic examinations were performed before and after the injection. The myocardium and the LV lumen were separated by endocardium that was visible before the treatment (Fig. 1Aa). After BR14 injection, the myocardium and the LV cavity showed comparable echo intensities, and the boundary between them was unclear (Fig. 1Ab). The hearts of the mice were sonicated under several conditions. After continuous sonication at 2.0 W/cm^2 and 50% PDR (2.0 W/50% PDR) for 60 s, most of the BR14 was disrupted, while a few residual circulating microbubbles were seen in the ventricle (Figs. 1Ac and Ad, arrowheads). The echocardiographic appearance subsequently became normal thereafter (data not shown).

Electrocardiographic examination was also performed to assess the influence of sonotransfection on the murine heart. Arrhythmia was seen in the mice exposed to ultrasound at 2.0 W/50% PDR after pDNA and BR14 had been injected into the LV, but they all quickly recovered from the same. Fig. 1B shows representative ECG changes before, during, and after the manipulation. Compared with the ECG profile before sonication (Fig. 1Ba), the QRS complex was prolonged immediately after the initiation of the ultrasound exposure (Fig. 1Bb). Thirty seconds later, the mice showed atrioventricular (AV) block (Fig. 1Bc), which persisted thereafter (Fig. 1Bd). Two minutes after termination of the sonication, the heart rate suddenly recovered to baseline (Figs. 1Be and Bf). In other cases, the AV block continued for shorter periods, ranging from 10 s to 2 min.

Echocardiographic analyses were performed to evaluate the LV contractility before and after sonoporation-mediated transfection (LV method, 2.0 W/50% PDR). As shown in Table 1, no significant change was observed for the parameters, Dd, Ds, IVS, PW, FS, and EF. The results indicated that the contractility of LV was not affected, even though its apex was punc-

Table 1
Echocardiographic analyses at pre- and post-sonoporation

	Pre-transfection ($n = 5$)	Post-transfection ($n = 5$)	P
BW (g)	22.8 ± 0.37	22.8 ± 0.20	ns
IVSTd (mm)	0.54 ± 0.02	0.60 ± 0.03	ns
PWTd (mm)	0.62 ± 0.02	0.58 ± 0.02	ns
LVIDd (mm)	3.24 ± 0.02	3.28 ± 0.05	ns
LVIDs (mm)	2.34 ± 0.04	2.40 ± 0.06	ns
EF (%)	60.8 ± 2.15	61.0 ± 1.90	ns
FS (%)	26.8 ± 1.39	27.0 ± 1.27	ns

Cardiac function was not significantly affected by sonoporation-mediated transfection of pDNA/BR14. M-mode echocardiographic analysis was performed on mice before and 4 days after sonoporation at 2.0 W/50% PDR. BW, body weight; IVSTd, interventricular septum thickness; PWTd, LV posterior wall thickness; LVIDd, LV internal dimensions at end diastole; LVIDs, LV internal dimensions at end systole; EF, ejection fraction; FS, fractional shortening. Data are expressed as means ± SE.

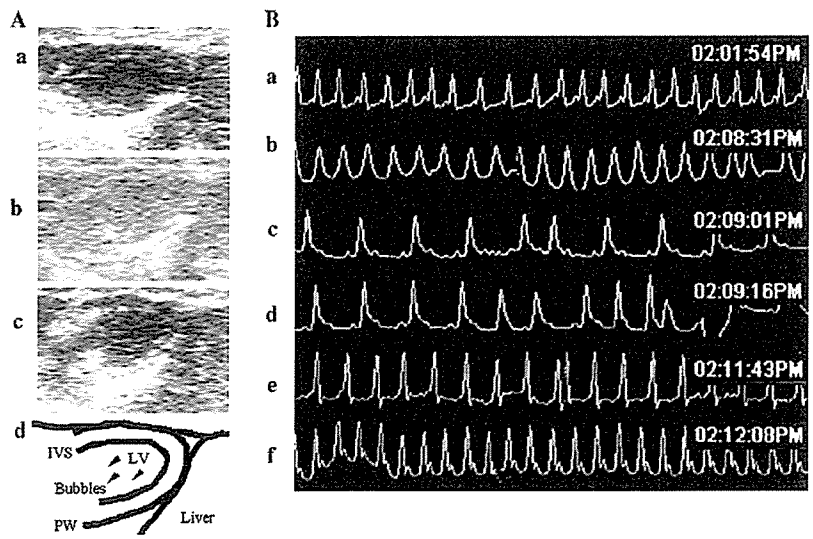

Fig. 1. (A) BR14 microbubbles were mostly disrupted by sonoporation, while some remained intact. C57BL/6 mice were injected with pGEG.GL3/BR14 into the LV. Shown are representative echocardiographic images before (a), immediately after (b), and 60 s after (c) the sonication at 2.0 W/50% PDR, while an echocardiographic image of (c) is illustrated schematically in (d). IVS, interventricular septum; PW, posterior wall. Arrowheads, intact microbubbles. (B) The transient arrhythmia caused by sonoporation. Mice received LV injection with pGEG.GL3/BR14, and sonoporation at 2.0 W/50% PDR was performed. Shown are representative ECG records before (a), and 0 s (b), 30 s (c), 45 s (d), 3 min (e), and 3.5 min (f) after the initiation of sonoporation.

tured on injection. The body weight of the mice did not significantly change following the sonoporation-mediated transfection.

Sonoporation remarkably facilitated cardiac gene transfer in mice

A mixture of pGEG.GL3 and BR14 was injected into the mice via their TV or LV. Ultrasound was directed at the chest at various output intensities and PDRs, and 2–7 days later Luc activity in the heart was measured. Representative data are shown in Fig. 2. When the mixture was injected into the LV, sonication at 2.0 W/50% PDR induced a significantly higher Luc activity on day 4 compared with that at 1.0 W/20% PDR (approximately 46-fold) or 1.0 W/50% PDR (approximately 13-fold). Transfection into the heart was more efficient when the mixture was injected into the LV than when it was injected into the TV. For example, compared with injection into the TV, expression was 67-fold higher 4 days following injection into the LV with sonoporation at 2.0 W/50% PDR. Optimal transfection was achieved by intra-LV injection and ultrasonication at 2.0 W/50% PDR, which resulted in Luc activity as high as approximately 6.0×10^4 RLU/mg protein/10 s on day 4, although the transgene activity was significantly decreased by day 7.

Transgene product was predominantly detected at subendocardial layer of the myocardium and anterior-septal wall of LV

To identify the localization of expression of the transferred gene, the heart was transfected with pGEG.β or pGEG.EGFP under the optimal conditions determined as described above. X-gal staining of the pGEG.β-transfected heart demonstrated that the β-gal was significantly expressed in the subendocardial layer of the LV and a part of the right ventricle. The strongest expression was detected at the anterior-septal wall of the LV that had faced the ultrasound probe (Fig. 3B). The pGEG.EGFP-transfected heart was examined histologically by fluorescence microscopy. The green fluorescence was observed in cardiomyocytes in the subendocardial layer (Figs. 3D and F). Consistent results were obtained by immunohistochemical staining of the pGEG.EGFP-transfected heart (data not shown). These findings indicated that transgene product was expressed in the subendocardial layer as well as in the anterior-septal wall of the LV.

Heart-specific transfection was achieved by sonoporation-based gene delivery

To investigate whether the present protocol allowed gene transfection in organs other than the heart, pGEG.GL3 was transfected as described above and the levels of Luc activity were determined quantitatively in lung, liver, kidney, spleen, intestine, ovary, and brain. Luc activity was not significantly increased in any of the organs tested (Fig. 4), indicating that the transfection procedure could deliver genes only to the heart.

Sonotransduction of siRNA induced specific gene silencing in coronary artery

We investigated whether the sonoporation-assisted DNA delivery procedure is also applicable to delivering siRNA into the heart. siRNA duplex specific for EGFP is capable of silencing the fluorescent protein in vivo, as demonstrated by preliminary experiments in which the siRNA was injected intravenously into EGFP TGM

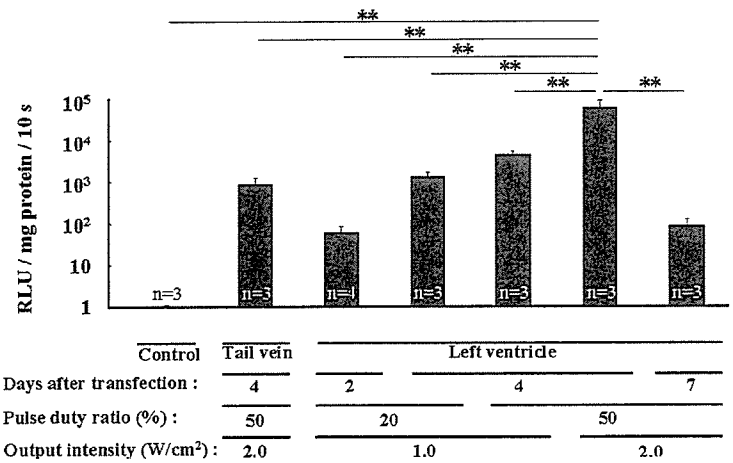

Fig. 2. Ultrasound-mediated transfection of pDNA under various conditions. pGEG.GL3/BR14 solution was injected into mice via the LV or TV route, and the heart was sonicated under the indicated conditions. Two, four, or seven days later, mice were sacrificed and Luc activities in the heart extracts were measured. Bars, SE. $^{**}P < 0.01$.

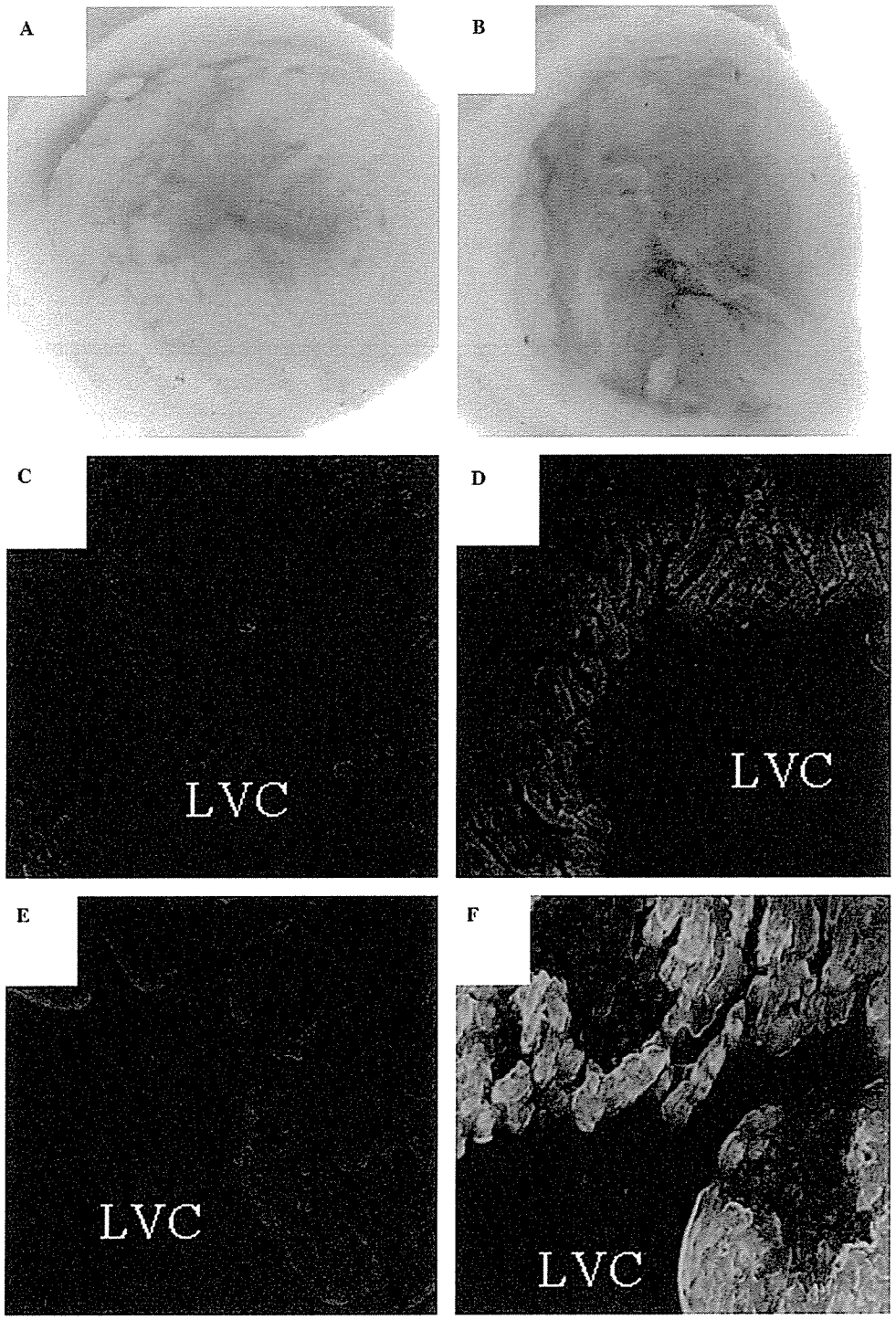

Fig. 3. Expression of transgene product in cardiomyocytes at the subendocardial layer and anterior-septal wall. Mice were given an intra-LV injection with pGEG.β/BR14, and sonication was performed at 2.0 W/50% PDR (B, D, and F). Control mice were left untreated (A, C, and E). Four days after the transfection, the hearts were excised. Shown are stereomicroscopic images of X-gal-stained cross-sections (A,B) and fluorescence microscopic images of cryosections (C–F). LVC, left ventricular cavity. Original magnifications were 4× (A,B), 40× (C,D), and 100× (E,F).

and expression of the transgene product was substantially suppressed in the hepatic parenchymal cells (Fig. 5B). siRNA was transfected into EGFP TGM, and the heart sections were observed by a fluorescence microscope. Representative findings are shown in Figs. 5C–F. In the control mice that received an injection of BR14 but not siRNA, the sonoporation procedure failed to affect EGFP expression in cardiomyocytes or coronary

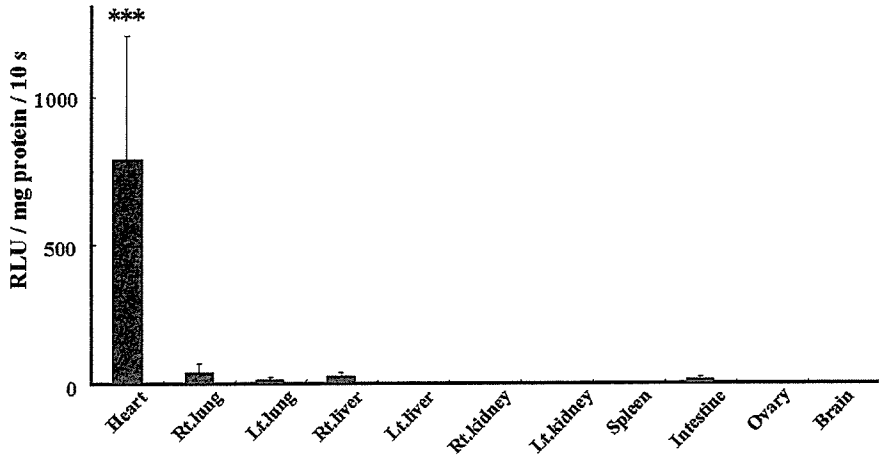

Fig. 4. Heart-specific pDNA transfer obtained by sonoporation-mediated transfection. Mice received an injection of pGEG.GL3/BR14 into the LV, and sonication was performed at 1.0 W/20% PDR. Four days later, the indicated organs were excised and Luc activity in each tissue extract was measured. Bars, SE. $***P < 0.001$ vs other organs ($n = 3$).

vessels (Figs. 5C and E). Intra-LV co-injection of siRNA-GFP and BR14 in combination with sonication at 1.0 W/10% PDR resulted in a substantial reduction of EGFP expression in the coronary artery wall 48 h after transduction, while cardiomyocytes were not influenced in terms of the intensity of the green fluorescence (Figs. 5D and F). The silencing of EGFP expression was detected not only at the main trunk of the left and right coronary arteries, but also at peripheral branches of the coronary arterial wall that could be identified by the structure of their vascular lumen. Similar results were also obtained by sonoporation performed under two other conditions, i.e., 1.0 W/10% PDR and 2.0 W/50% PDR (data not shown).

Discussion

Intra-LV injection of a mixture of an expression vector and the micobubble agent BR14 and concomitant ultrasonication resulted in significant expression of the marker gene in cardiomyocytes in the subendocardial layer and the antero-septal wall of the murine heart. BR14 also facilitated sonoporation-mediated transfer of siRNA duplex into the coronary artery, resulting in substantial gene silencing in vivo. Our study suggests an improved methodology for achieving safe and efficient genetic modification in the heart, in both gain-of-function and loss-of-function manners.

The present study also indicates that sonoporation-mediated pDNA transfer is strongly enhanced by the third-generation microbubble, BR14. BR14 is a negatively charged ultrasound contrast agent consisting of perfluorobutane-containing microbubbles stabilized by a phospholipid monolayer [20,34,35]. We also compared BR14 with Optison in sonoporation-mediated transfection into murine heart. An intra-TV injection of 500 μg pGEG.GL3/Optison and sonoporation at 2.0 W/50% PDR resulted in Luc expression in the cardiac muscle at a level similar to that when BR14 was used (1330 ± 310 RLU/mg protein/10 s on day 4 ($n = 9$)). However, some mice died immediately after receiving an intra-TV injection of Optison even without the sonoporation. Although Optison has been shown to be a useful agent for ultrasound-based transfection in rats and larger animals [9,12–14,17,18], BR14 may be more suitable in mice because a TV injection of BR14 did not kill any mice in the present study. The difference in results may be due to difference in the size of the agents: the mean diameter of BR14 is 2.5–3.0 μm, which is small compared with its predecessors [17,35,36]. The diameter of erythrocytes in C57BL/6 mice is about a half of that in humans (MCV 44.8 ± 0.26 fl, MCH 15.6 ± 0.49 pg, MCHC 34.7 ± 1.12 g/dl). Fisher et al. [36] examined the distribution of microbubbles intravenously administered into C57BL-6 mice. Intravital microscopic analyses demonstrated that neutral microbubbles larger than 4 μm in diameter persisted in capillaries in a size-dependent manner. Although the mean diameter of Optison is 2.0–4.5 μm, it contains bubbles up to 32 μm in diameter. These large bubbles may cause lethal embolisms in some vital organs in mice.

With regard to the routes of injection of pDNA/BR14, a higher rate of pDNA transfection was obtained by injection into the LV than by injection into the TV. These results suggest that high concentrations of pDNA and microbubble in coronary circulation are required at the time of sonication to achieve efficient sonoporation-based transfection.

In our study, pDNA could have reached the myocardium via 2 routes, i.e., directly from the LV cavity or through the coronary capillaries. This may explain why pDNA was predominantly delivered into the myocardium in the subendocardial layer and the anterior-septal

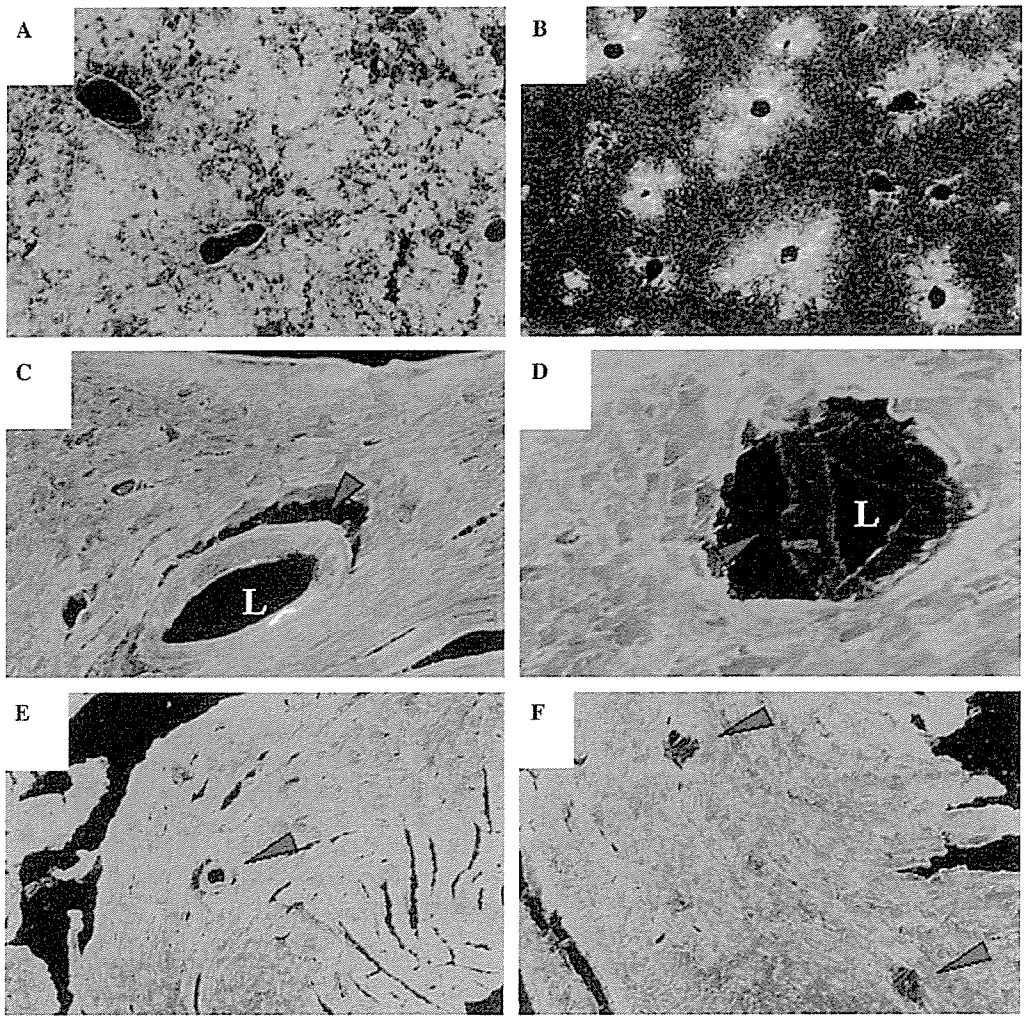

Fig. 5. Sonoporation-based transduction of siRNA silenced EGFP expression in the coronary arterial wall. (A) Fluorescence microscopic image of a liver section of EGFP-TGM. (B) EGFP-TGM were given a rapid tail vein injection with siRNA-GFP. Two days later, cryosections of the liver were observed under fluorescence microscope. (C–F) EGFP-TGM received an intra-LV injection of BR14 (C,E) or siRNA-GFP/BR14 (D,F), and sonication was performed at 1.0 W/10% PDR. Two days later, cryosections of the heart were observed under fluorescence microscope. Arrowheads in (C,D) indicate the left coronary artery, while those in (E,F) indicate the septal branches. L, lumen of arteries. Original magnifications were 100× (A,B), 200× (C,D), and 40× (E,F).

wall. Chen et al. [16] showed that the rate of pDNA transfection was significantly diminished by destroying microbubbles in the LV cavity before their entrance into the coronary microcirculation. So, presumably, the quantity of the pDNA transported via the coronary capillaries was greater than that delivered directly through the LV.

The present results showed that cardiomyocytes in the anterior-septal wall expressed the transgene more strongly than those in the inferior-posterior wall. The ultrasound beam is probably attenuated during passage through the cardiac muscle layers, so that the transfection efficiency may be inversely proportional to the distance from the probe. These results are consistent with the report by Chen et al. [16], who demonstrated that gene expression in the anterior wall was 2- to 2.5-fold greater than that in the posterior wall in rat heart transfected with pDNA by their sonoporation-mediated transduction protocols.

In the present study, maximum expression of transgene was obtained 4 days after transfection. This is consistent with a previous study in which expression levels peaked on day 4 following sonoporation-mediated transfer of pDNA and Optison into rat hearts [15].

In some previous studies, ultrasound-mediated destruction of Optison and other microbubbles induced rupture of microvessels at the sonicated site of the target organs [37,38]. In our experiments, a careful microscopic study did not demonstrate the RBC extravasation into the myocardium (data not shown). This is consistent

with echocardiographic examinations which demonstrated that cardiac contractility was not significantly affected after sonoporation (Table 1).

Some previous studies indicated that RNAi was induced in vitro into rat cardiomyocytes [39] as well as in human coronary vascular smooth muscle cells [40] in culture. We also demonstrated successful sequence-specific knockdown of endogenous gene expression in vivo in the coronary artery of adult mice using siRNA. RNAi may offer novel strategies for therapeutic molecular targeting, enabling artificial regulation of proteins that are responsible for the pathogenesis and/or progression of coronary diseases. For example, specific silencing of NF-κB or platelet-derived growth factor (PDGF) A-chain may suppress neointimal formation in coronary vasculature, which may have prophylactic implications for restenosis after coronary intervention as well as for the progression of atherosclerosis. These concepts are supported by previous studies in which balloon-injured artery models of animals were treated with decoy oligonucleotide that suppresses NF-κB activity [41] or a PDGF-targeting ribozyme [42].

It is noteworthy that pDNA was transfected effectively into cardiomyocytes, while the siRNA was transduced into coronary vascular wall. Although the precise mechanisms underlying these phenomena remain unclear, we propose the following explanation. Ultrasound-mediated cavitation may damage endothelial cells in both arteries and capillaries. Due to its small size, siRNA may easily diffuse from the bloodstream into tissue via endothelium when passing through the coronary arteries and arterioles, resulting in efficient transduction into arterial/arteriolar walls including the smooth muscle cells. Because pDNA permeates endothelium more slowly, transduction occurs less readily during its passage through arterioles. Instead, the pDNA is transduced predominantly at the capillary bed where cavitation from transient microbubbles is more intense. As a result, pDNA may be transfected into cardiomyocytes residing immediately beyond the extremely thin capillary wall.

To obtain further higher transduction efficacy, the following may be employed in combination with the sonoporatoin. Administration with the vascular endothelial growth factor (VEGF) may facilitate transfer of genetic materials through the endothelium, due to an increase in permeability of the endothelial cell membrane [43]. ECG-triggered sonication may also be effective because ultrasound-based cavitation can be generated precisely at the diastolic phase, when the coronary blood flow is higher than in the systolic phase. Use of RNase inhibitor [25] may prevent degradation of siRNA.

Kunichika et al. [20] showed that BR14 highlights ischemic risk areas in myocardium as a hyperenhanced "hot spot" when myocardial contrast echocardiography is performed following coronary reperfusion. Therefore, sonoporation using BR14 may enable targeted gene delivery to ischemic cardiomyocytes in patients with myocardial infarction, specifically delivering therapeutic nucleic acids into damaged cells.

Finally, it should be emphasized that the present procedure enables gene transfer and knockdown in the murine heart, although previous studies have documented ultrasound-assisted transfection into the hearts of larger animals, including rats [10,16] and dogs [11]. The mouse is a useful animal for post-genomic experimental cardiology. Particularly, a variety of transgenic and gene out mice have been established, providing extremely useful tools to elucidate the molecular mechanisms of cardiovascular disorders. The present method may be applied to these genetically engineered mice, providing a suitable technology to promote functional genomic analyses, as well as to examine candidate molecules for therapeutic molecular targeting for cardiovascular diseases.

Acknowledgment

This work was supported by a Grant-in-Aid for scientific research from the Japanese Ministry of Education, Culture, Sports, Science and Technology.

References

[1] M. Iwatate, Y. Gu, T. Dieterle, Y. Iwanaga, K.L. Peterson, M. Hoshijima, K.R. Chien, J. Ross, In vivo high-efficiency transcoronary gene delivery and Cre-LoxP gene switching in the adult mouse heart, Gene Ther. 10 (2003) 1814–1820.
[2] H.C. Champion, D. Georgakopoulos, S. Haldar, L. Wang, Y. Wang, D.A. Kass, Robust adenoviral and adeno-associated viral gene transfer to the in vivo murine heart: application to study of phospholamban physiology, Circulation 108 (2003) 2790–2797.
[3] K. Li, R.E. Welikson, K.L. Vikstrom, L.A. Leinwand, Direct gene transfer into the mouse heart, J. Mol. Cell. Cardiol. 29 (1997) 1499–1504.
[4] H. Lin, M.S. Parmacek, G. Morle, S. Bolling, J.M. Leiden, Expression of recombinant genes in myocardium in vivo after direct injection of DNA, Circulation 82 (1990) 2217–2221.
[5] R.N. Kitsis, P.M. Buttrick, E.M. McNally, M.L. Kaplan, L.A. Leinwand, Hormonal modulation of a gene injected into rat heart in vivo, Proc. Natl. Acad. Sci. USA 88 (1991) 4138–4142.
[6] K. Tomiyasu, Y. Oda, M. Nomura, E. Satoh, S. Fushiki, J. Imanishi, M. Kondo, O. Mazda, Direct intra-cardiomuscular transfer of beta2-adrenergic receptor gene augments cardiac output in cardiomyopathic hamsters, Gene Ther. 7 (2000) 2087–2093.
[7] K. Ogawa, K. Tachibana, T. Uchida, T. Tai, N. Yamashita, N. Tsujita, R. Miyauchi, High-resolution scanning electron microscopic evaluation of cell-membrane porosity by ultrasound, Med. Electron Microsc. 34 (2001) 249–253.
[8] D.L. Miller, S.V. Pislaru, J.E. Greenleaf, Sonoporation: mechanical DNA delivery by ultrasonic cavitation, Somat. Cell Mol. Genet. 27 (2002) 115–134.

[9] T. Li, K. Tachibana, M. Kuroki, M. Kuroki, Gene transfer with echo-enhanced contrast agents: comparison between Albunex, Optison, and Levovist in mice-initial results, Radiology 229 (2003) 423–428.
[10] R.V. Shohet, S. Chen, Y.T. Zhou, Z. Wang, R.S. Meidell, R.H. Unger, P.A. Grayburn, Echocardiographic destruction of albumin microbubbles directs gene delivery to the myocardium, Circulation 101 (2000) 2554–2556.
[11] M. Vannan, T. McCreery, P. Li, Z. Han, E. Unger, B. Kuersten, E. Nabel, S. Rajagopalan, Ultrasound-mediated transfection of canine myocardium by intravenous administration of cationic microbubble-linked plasmid DNA, J. Am. Soc. Echocardiogr. 15 (2002) 214–218.
[12] M. Blomley, Which US microbubble contrast agent is best for gene therapy? Radiology 229 (2003) 297–298.
[13] S. Miura, K. Tachibana, T. Okamoto, K. Saku, In vitro transfer of antisense oligodeoxynucleotides into coronary endothelial cells by ultrasound, Biochem. Biophys. Res. Commun. 298 (2002) 587–590.
[14] Y. Taniyama, K. Tachibana, K. Hiraoka, T. Namba, K. Yamasaki, N. Hashiya, M. Aoki, T. Ogihara, K. Yasufumi, R. Morishita, Local delivery of plasmid DNA into rat carotid artery using ultrasound, Circulation 105 (2002) 1233–1239.
[15] R. Bekeredjian, S. Chen, P.A. Frenkel, P.A. Grayburn, R.V. Shohet, Ultrasound-targeted microbubble destruction can repeatedly direct highly specific plasmid expression to the heart, Circulation 108 (2003) 1022–1026.
[16] S. Chen, R.V. Shohet, R. Bekeredjian, P. Frenkel, P.A. Grayburn, Optimization of ultrasound parameters for cardiac gene delivery of adenoviral or plasmid deoxyribonucleic acid by ultrasound-targeted microbubble destruction, J. Am. Coll. Cardiol. 42 (2003) 301–308.
[17] S. Mayer, P.A. Grayburn, Myocardial contrast agents: recent advances and future directions, Prog. Cardiovasc. Dis. 44 (2001) 33–44.
[18] R. Bekeredjian, P.A. Grayburn, R.V. Shohet, Use of ultrasound contrast agents for gene or drug delivery in cardiovascular medicine, J. Am. Coll. Cardiol. 45 (2005) 329–335.
[19] N.G. Fisher, H. Leong-Poi, T. Sakuma, S.J. Rim, J.P. Bin, S. Kaul, Detection of coronary stenosis and myocardial viability using a single intravenous bolus injection of BR14, J. Am. Coll. Cardiol. 39 (2002) 523–529.
[20] H. Kunichika, B. Peters, B. Cotter, H. Masugata, N. Kunichika, P.L. Wolf, A.N. DeMaria, Visualization of risk-area myocardium as a high-intensity, hyperenhanced "hot spot" by myocardial contrast echocardiography following coronary reperfusion: quantitative analysis, J. Am. Coll. Cardiol. 42 (2003) 552–557.
[21] Y. Sakakima, S. Hayashi, Y. Yagi, A. Hayakawa, K. Tachibana, A. Nakao, Gene therapy for hepatocellular carcinoma using sonoporation enhanced by contrast agents, Cancer Gene Ther. (in press).
[22] E.F. Akowuah, C. Gray, A. Lawrie, P.J. Sheridan, C.H. Su, T. Bettinger, A.F. Brisken, J. Gunn, D.C. Crossman, S.E. Francis, A.H. Baker, C.M. Newman, Ultrasound-mediated delivery of TIMP-3 plasmid DNA into saphenous vein leads to increased lumen size in a porcine interposition graft model, Gene Ther. 12 (2005) 1154–1157.
[23] G.J. Hannon, RNA interference, Nature 418 (2002) 244–251.
[24] J. Downward, RNA interference, Br. Med. J. 328 (2004) 1245–1248.
[25] A.P. McCaffrey, L. Meuse, T.T. Pham, D.S. Conklin, G.J. Hannon, M.A. Kay, RNA interference in adult mice, Nature 418 (2002) 38–39.
[26] D.L. Lewis, J.E. Hagstrom, A.G. Loomis, J.A. Wolff, H. Herweijer, Efficient delivery of siRNA for inhibition of gene expression in postnatal mice, Nat. Genet. 32 (2002) 107–108.
[27] T. Kishida, H. Asada, S. Gojo, S. Ohashi, M. Shin-Ya, K. Yasutomi, R. Terauchi, K.A. Takahashi, T. Kubo, J. Imanishi, O. Mazda, Sequence-specific gene silencing in murine muscle induced by electroporation-mediated transfer of short interfering RNA, J. Gene. Med. 6 (2004) 105–110.
[28] F.D. Cui, T. Kishida, S. Ohashi, H. Asada, K. Yasutomi, E. Satoh, T. Kubo, S. Fushiki, J. Imanishi, O. Mazda, Highly efficient gene transfer into murine liver achieved by intravenous administration of naked Epstein–Barr virus (EBV)-based plasmid vectors, Gene Ther. 8 (2001) 1508–1513.
[29] T. Kishida, H. Asada, Y. Itokawa, F.D. Cui, M. Shin-Ya, S. Gojo, K. Yasutomi, Y. Ueda, H. Yamagishi, J. Imanishi, O. Mazda, Interleukin (IL)-21 and IL-15 genetic transfer synergistically augments therapeutic antitumor immunity and promotes regression of metastatic lymphoma, Mol. Ther. 8 (2003) 552–558.
[30] H. Nakanishi, O. Mazda, E. Satoh, H. Asada, H. Morioka, T. Kishida, M. Nakao, Y. Mizutani, A. Kawauchi, M. Kita, J. Imanishi, T. Miki, Nonviral genetic transfer of Fas ligand induced significant growth suppression and apoptotic tumor cell death in prostate cancer in vivo, Gene Ther. 10 (2003) 434–442.
[31] O. Mazda, Improvement of nonviral gene therapy by Epstein–Barr virus (EBV)-based plasmid vectors, Curr. Gene. Ther. 2 (2002) 379–392.
[32] S. Ohashi, T. Kubo, T. Kishida, T. Ikeda, K. Takahashi, Y. Arai, R. Terauchi, H. Asada, J. Imanishi, O. Mazda, Successful genetic transduction in vivo into synovium by means of electroporation, Biochem. Biophys. Res. Commun. 293 (2002) 1530–1535.
[33] K. Tomiyasu, E. Satoh, Y. Oda, K. Nishizaki, M. Kondo, J. Imanishi, O. Mazda, Gene transfer in vitro and in vivo with Epstein–Barr virus-based episomal vector results in markedly high transient expression in rodent cells, Biochem. Biophys. Res. Commun. 253 (1998) 733–738.
[34] H. Takeuchi, K. Ohmori, I. Kondo, K. Shinomiya, A. Oshita, Y. Takagi, J. Yoshida, K. Mizushige, M. Kohno, Interaction with leukocytes: phospholipid-stabilized versus albumin-shell microbubbles, Radiology 230 (2004) 735–742.
[35] N.G. Fisher, J.P. Christiansen, H. Leong-Poi, A.R. Jayaweera, J.R. Lindner, S. Kaul, Myocardial and microcirculatory kinetics of BR14, a novel third-generation intravenous ultrasound contrast agent, J. Am. Coll. Cardiol. 39 (2002) 530–537.
[36] N.G. Fisher, J.P. Christiansen, A. Klibanov, R.P. Taylor, S. Kaul, J.R. Lindner, Influence of microbubble surface charge on capillary transit and myocardial contrast enhancement, J. Am. Coll. Cardiol. 40 (2002) 811–819.
[37] D.L. Miller, J. Quddus, Diagnostic ultrasound activation of contrast agent gas bodies induces capillary rupture in mice, Proc. Natl. Acad. Sci. USA 97 (2000) 10179–10184.
[38] R.J. Price, D.M. Skyba, S. Kaul, T.C. Skalak, Delivery of colloidal particles and red blood cells to tissue through microvessel ruptures created by targeted microbubble destruction with ultrasound, Circulation 98 (1998) 1264–1267.
[39] A. Watanabe, M. Arai, M. Yamazaki, N. Koitabashi, F. Wuytack, M. Kurabayashi, Phospholamban ablation by RNA interference increases Ca^{2+} uptake into rat cardiac myocyte sarcoplasmic reticulum, J. Mol. Cell. Cardiol. 37 (2004) 691–698.
[40] F. Blaschke, D. Bruemmer, F. Yin, Y. Takata, W. Wang, M.C. Fishbein, T. Okura, J. Higaki, K. Graf, E. Fleck, W.A. Hsueh, R.E. Law, C-reactive protein induces apoptosis in human coronary vascular smooth muscle cells, Circulation 110 (2004) 579–587.
[41] K. Yamasaki, T. Asai, M. Shimizu, M. Aoki, N. Hashiya, H. Sakonjo, H. Makino, Y. Kaneda, T. Ogihara, R. Morishita, Inhibition of NFkappaB activation using cis-element 'decoy' of NFkappaB binding site reduces neointimal formation in porcine balloon-injured coronary artery model, Gene Ther. 10 (2003) 356–364.

[42] M. Kotani, N. Fukuda, H. Ando, W.Y. Hu, S. Kunimoto, S. Saito, K. Kanmatsuse, Chimeric DNA–RNA hammerhead ribozyme targeting PDGF A-chain mRNA specifically inhibits neointima formation in rat carotid artery after balloon injury, Cardiovasc. Res. 57 (2003) 265–276.

[43] P. Gregorevic, M.J. Blankinship, J.M. Allen, R.W. Crawford, L. Meuse, D.G. Miller, D.W. Russell, J.S. Chamberlain, Systemic delivery of genes to striated muscles using adeno-associated viral vectors, Nat. Med. 10 (2004) 828–834.

Granulocyte Colony-Stimulating Factor–Mobilized Circulating c-Kit+/Flk-1+ Progenitor Cells Regenerate Endothelium and Inhibit Neointimal Hyperplasia After Vascular Injury

Michitaka Takamiya, Mitsuhiko Okigaki, Denan Jin, Shinji Takai, Yoshihisa Nozawa, Yasushi Adachi, Norifumi Urao, Kento Tateishi, Tetsuya Nomura, Kan Zen, Eishi Ashihara, Mizuo Miyazaki, Tetsuya Tatsumi, Tomosaburo Takahashi, Hiroaki Matsubara

Background—Granulocyte colony-stimulating factor (G-CSF) treatment was shown to inhibit neointimal formation of balloon-injured vessels, whereas neither the identification of progenitor cells involved in G-CSF–mediated endothelial regeneration with a bone marrow (BM) transplant experiment nor the functional properties of regenerated endothelium have been studied.

Methods and Results—Recombinant human G-CSF (100 μg/kg per day) was injected daily for 14 days starting 3 days before balloon injury in the rat carotid artery. Neointimal formation of denuded vessels on day 14 was markedly attenuated by G-CSF (39% versus the control; $P<0.05$). Endothelial cell–specific immunostaining revealed an enhancement of re-endothelialization (1.8-fold increase versus the control; $P<0.05$) and inhibition of extravasation of Evans Blue dye (47%; $P=0.02$). The regenerated endothelium exhibited acetylcholine-mediated vasodilatation in NO-dependent manner. G-CSF increased the circulating c-Kit+/Flk-1+ cells (9.1-fold; $P<0.02$), which showed endothelial properties in vitro (acetylated low-density lipoprotein uptake and lectin binding) and incorporated into the regenerated endothelium in vivo. A BM replacement experiment with green fluorescent protein (GFP)–overexpressing cells showed that BM-derived GFP+/CD31+ endothelial cells occupied 39% of the total luminal length in the G-CSF–mediated neo-endothelium (2% in the control).

Conclusion—The G-CSF–induced mobilization of BM-derived c-Kit+/Flk-1+ cells contributes to endothelial regeneration, and this cytokine therapy may be a feasible strategy for the promotion of re-endothelialization after angioplasty. (*Arterioscler Thromb Vasc Biol.* **2006;26:751-757.**)

Key Words: restenosis ■ endothelium ■ carotid artery ■ cytokines ■ vascular biology

Endothelial cells (ECs) cover the luminal surface of blood vessels and maintain multiple vascular functions. The disruption of endothelial coverage causes a decrease in the production of vasculoprotective mediators such as NO, leading to elevated vascular tonus, enhanced inflammation, and medial smooth muscle cell proliferation. The resultant neointimal hyperplasia causes restenosis after angioplasty.[1]

Bone marrow (BM)–derived endothelial progenitor cells (EPCs) was isolated from the mononuclear cell (MNC) population in the peripheral blood (PB).[2,3] Transplantation of autologous circulating EPCs (CEPCs) to balloon-denuded arteries was reported to induce rapid re-endothelialization of the injured artery.[4,5] Moreover, transfusion of spleen-derived EPCs or EPCs overexpressing endothelial NO synthase reduced neointimal formation after vascular injury.[6,7] Delivery of cultured PB-MNCs to balloon-injured arteries accelerated re-endothelialization associated with endothelium-dependent vasoreactivity and reduced neointimal formation.[7]

Cytokines efficiently mobilize hematopoietic precursor cells from BM.[8] Takahashi et al showed that exogenous granulocyte/macrophage colony-stimulating factor (CSF) mobilize CEPCs from BM and thereby contributes to neovascularization of ischemic tissues.[9] Recently, granulocyte-CSF (G-CSF) was shown to recruit BM-derived EPCs[10] and enhance the BM cell mobilization to brain, leading to angiogenesis and eventually a reduction in the volume of cerebral infarction.[11] G-CSF was also reported to increase angiogenesis in the BM of G-CSF–treated patients.[12] Treatment with

Original received June 6, 2005; final version accepted December 15, 2005.

From the Department of Cardiovascular Medicine (M.T., M.O., N.U., K.T., T.N., K.Z., E.A., T. Tatsumi, T. Takahashi, H.M.), Kyoto Prefectural University School of Medicine, Japan; Department of Pharmacology (D.J., S.T., M.M.), Osaka Medical College, Takatsuki, Japan; Pharmacobioregulation Research Laboratory (Y.N.), Taiho Pharmaceutical Co. Ltd, Saitama, Japan; and Department of Pathology II (Y.A.), Kansai Medical University, Moriguchi, Japan.

Correspondence to Mitsuhiko Okigaki MD, Department of Cardiovascular Medicine, Kyoto Prefectural University of Medicine, Kamigyo-ku, Kyoto, 602-8566, Japan. E-mail okigakim@koto.kpu-m.ac.jp

Arterioscler Thromb Vasc Biol. **is available at http://www.atvbaha.org** **DOI: 10.1161/01.ATV.0000205607.98538.9a**

G-CSF plus macrophage CSF accelerates neovascularization in limb ischemia.[13] G-CSF enhances endothelialization of small-caliber prosthetic implanted grafts,[14,15] and intracoronary infusion of G-CSF–mobilized PB-MNCs improved cardiac regional flow in patients with myocardial infarction.[16] Kong et al reported that mobilization of CEPCs by exogenous G-CSF facilitates re-endothelialization and inhibits neointimal development,[17] whereas the cell types of BM-derived cells contributing to G-CSF–mediated endothelial regeneration in the vascular repair model has not been defined in a BM transplant experiment, and neither the involvement of G-CSF–mediated outgrowth of resident ECs bordering the injured area nor the functional properties of the regenerated endothelium were studied in G-CSF–treated animals. To further elucidate these undetermined issues, the present study was designed, and it provided the additional novel findings that: (1) BM-derived c-Kit+/Flk-1+ progenitor cells mobilized by G-CSF directly contribute to the endothelial regeneration after EC-denuded injury and can differentiate to EC-like cells in vitro, (2) the contribution of the G-CSF–mediated outgrowth of resident ECs is negligible, and (3) the repaired artery showed NO-mediated arterial relaxation and inhibition of neointimal hyperplasia. These findings suggested that G-CSF therapy can be a feasible therapy to inhibit neointimal hyperplasia after angioplasty.

Materials and Methods

Balloon Injury Model

A 2Fr Fogarty arterial embolectomy catheter (Edwards Lifesciences) was inserted into the right common carotid artery of Lewis rats (LEW/SsN Slc; 10 to 12 weeks of age) and inflated 3 times with 300 μL of air. Human G-CSF (Lenograstim; 10, 30, or 100 μg/kg per day) or vehicle (saline) was subcutaneously injected daily for 14 days from 3 days before injury. The lesion was harvested on day 14. Green fluorescent protein (GFP) transgenic mice were generously donated by Dr Okabe (Osaka University, Japan).[18] All experimental procedures complied with the institutional guidelines for animal experiments.

Morphometric Analysis

The injured lesion was fixed with 4% paraformaldehyde, paraffin sectioned, and stained with hematoxylin and eosin or Elastica van Gieson. Three sections from each carotid artery at 300-μm intervals were analyzed with NIH image software. The absolute intimal area or relative ratio of intimal-to-medial area (I/M ratio) was evaluated. Evans blue dye (5%; Sigma) was transfused to rats 10 minutes before euthanasia to identify the remaining denuded area. Furthermore, to analyze the EC-recovered area, samples were incubated with horseradish peroxidase (HRP)–conjugated anti-FactorVIII antibody, followed by visualization with 3, 3′-diaminobenzidine (DAB). Slides were then counterstained with hematoxylin.

Functional Assay of Regenerated Endothelium

NO-mediated vasorelaxation of regenerated endothelium was evaluated as we described previously.[5]

Transfusion of G-CSF–Induced PB-MNCs

PB-MNCs were isolated by Percoll gradient centrifugation (Lymphoprep; NYCOMED) from 5-day G-CSF–treated donor rats and labeled with DiI[19] and transfused to the recipient Lewis rat after arterial injury (1×10^7 cells). After a 5-day G-CSF treatment in GFP-overexpressing mice, PB-MNCs were prepared and incubated with phycoerythrin (PE)–Cy5-conjugated anti-mouse CD45 or anti-mouse c-Kit antibodies (BD Pharmingen), as well as PE-conjugated anti-mouse Flk-1 (Becton Dickinson). GFP+/c-Kit+/Flk-1+ and GFP+/c-Kit+/Flk-1− cells were sorted and transfused to the recipient nude rats (F344/N rnu/rnu) after arterial injury. On day 14, the lesion was frozen sectioned and incubated with anti-CD31 antibody (Santa Cruz Biotechnology), followed by rhodamine-conjugated secondary antibody (DAKO).

Primary Culture of G-CSF–Induced PB-MNCs

PB-MNCs were prepared from 5-day G-CSF–treated rats and cultured on fibronectin-coated chamber slides (Becton Dickinson) for 7 days with 10% FBS-DMEM (GIBCO). Adherent cells were incubated with 2.4 μL/mL of DiI-labeled acetylated LDL (Molecular Probes) for 120 minutes, fixed with 2% paraformaldehyde, and stained with 10 ng/mL of fluorescein isothiocyanate (FITC)–conjugated Ulex europaeus agglutinin-1 (UEA-1) lectin (Sigma). The double fluorescent cells were counted in 4 randomly selected high-power fields.

Fluorescence-Activated Cell Sorter Analysis of G-CSF–Induced Mice PB-MNCs

PB-MNCs were prepared from 5-day G-CSF–treated C57BL/6 mice, incubated with PE-conjugated antibody against CD3, CD8, B220, CD11b, Ter119 or Gr-1, and FITC-conjugated anti-CD34 antibody as well as biotin-conjugated mouse antibody against Flk-1 or c-Kit, followed by activated protein C–conjugated secondary antibody (all from Pharmingen). Samples were analyzed with fluorescent-activated cell sorter (FACS) caliber using Cell Quest (Becton Dickinson).

BM Transplantation

1×10^7 BM cells from GFP-overexpressing mice were transplanted to nude rats (F344/N rnu/rnu) after 6 Gray irradiation. At week 4, arterial injury was conducted, and G-CSF (100 μg/kg per day) was injected daily for 14 days from 3 days before arterial injury. The lesions were frozen sectioned and stained with anti-CD31 antibody with rhodamine-conjugated secondary antibody (DAKO).

Immunohistochemistry

The injured lesions were paraffin sectioned at 14 days after balloon injury and immunostained with anti-rat CD45 (BD Pharmingen) and rat cross-reactive anti–interleukin-1β (IL-1β) antibodies (sc-7884; Santa Cruz Biotechnology) and HRP-conjugated secondary antibody, followed by visualization with DAB and counterstained with hematoxylin.

Statistical Analysis

Statistical analyses were performed with 1-way ANOVA followed by pairwise contrasts using Dunnett test. Data (means±SE) were considered statistically significant when P was <0.05.

Results

G-CSF Inhibits Neointimal Hyperplasia After Arterial Injury

We determined whether G-CSF treatment inhibits neointimal hyperplasia after EC-denuded balloon injury of carotid artery. Neointimal lesions developed in the vehicle-treated vessels 2 weeks after injury, whereas G-CSF treatment markedly reduced the neointimal formation in a dose-dependent manner (10 to 100 μg/kg per day; Figure 1). Morphometric analysis revealed a remarkable decrease in the neointimal area of high-dose G-CSF (100 μg/kg per day)–treated rats compared with the vehicle-treated group (39±3% decrease; n=10; $P<0.05$). The I/M ratio in G-CSF–treated rats was less than that in the vehicle-treated group (46.0±7.6% versus 84.3±7.3%; n=10; $P<0.05$; Figure 1B). Thus, it is unlikely that G-CSF directly affects the outgrowth of resident smooth

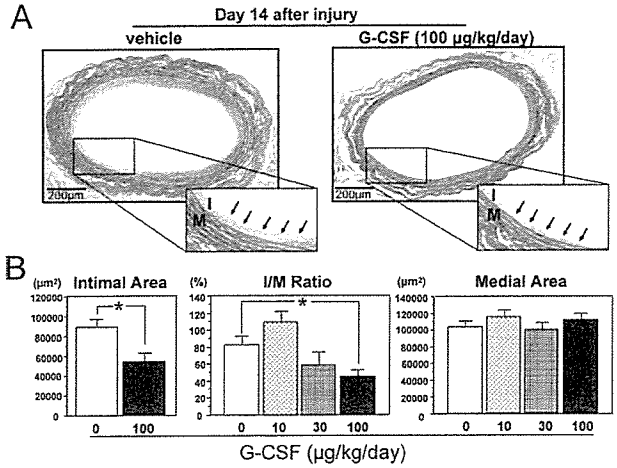

Figure 1. G-CSF inhibits neointimal hyperplasia after EC-denuded balloon injury. Endothelial denudation of rat carotid artery was induced by balloon catheter (day 0). The rats were injected with G-CSF: 0 μg/kg per day (vehicle only), 10, 30, or 100 μg/kg per day (n=10, each group). A, G-CSF (100 μg/kg per day) was subcutaneously injected daily for 14 days from 3 days before arterial injury. On day 14, the injured lesion was stained with Elastica van Gieson and subjected to morphometrical analysis. Arrows indicate apparent neointimal hyperplasia in the vehicle-injected group and marked inhibition of neointimal lesions in the G-CSF–treated group. B, Statistical analysis: intimal (I) or medial area (M) as well as the I/M ratio were evaluated 14 days after balloon injury with NIH image software. *$P<0.05$ vs vehicle-injected groups (n=10).

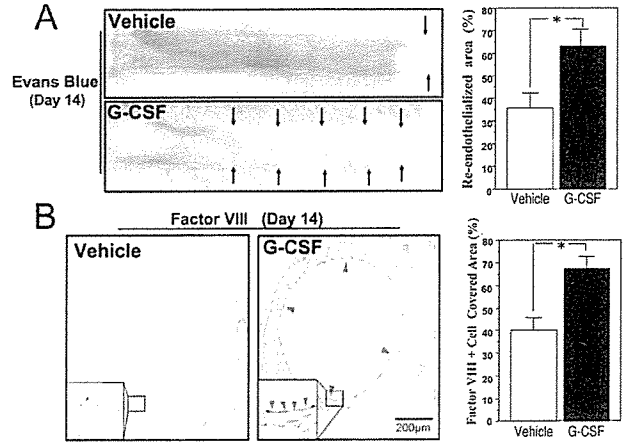

Figure 2. G-CSF facilitates re-endothelialization after EC-denuded injury. A, At 14 days after balloon injury, Evans blue dye was intravenously injected before euthanization. The re-endothelialized area, which appears white (arrows), was significantly larger in the G-CSF group than in the vehicle-treated group. *$P<0.05$ vs vehicle-injected group (n=6). B, On day 14, the injured lesion was immunostained with HRP-conjugated anti-FactorVIII antibody, followed by visualization with DAB. The FactorVIII+ cell-covered area (arrowheads) to the total length of luminal surface (%) in the G-CSF–treated group was significantly greater than in the vehicle-injected group. *$P<0.05$ vs vehicle-treated group (n=6).

muscle cells in the injured artery in vivo, although G-CSF was reported to stimulate the growth of the cultured vascular smooth muscle cells.[20]

We also studied whether G-CSF aggravated inflammatory cell infiltration and cytokine expression in the injured arteries by examining the infiltration of inflammatory cells (CD45+ cells) and the expression of inflammatory cytokine (IL-1β) in the injured arteries. Figure I (available online at http://atvb.ahajournals.org) shows that the infiltration of CD45+ cells and the expression of IL-1β are markedly inhibited in the day-14 neoendothelium of G-CSF–treated rats compared with those in the saline-treated controls, consistent with the previous observation that G-CSF pellet–induced angiogenic activity on the cornea occurred without any sign of inflammatory reactions.[21]

G-CSF treatment dose dependently (10, 30, and 100 μg/kg per day) elevated the number of white blood cells 14 days after treatment (14 500±2000, 19 660±430, 33 520±2171 cells; n=15 each), which were significantly higher compared with the vehicle-injected control (3640±153; n=15; $P<0.01$). Any dose of G-CSF (10, 30, or 100 μg/kg per day) did not affect the survival rate and body weight of the administrated rats and did not cause any macroanatomic change. Because 100 μg/kg per day of human G-CSF used here is considered to be similar to the human clinical dose based on the species difference between human and rodents,[22] and therefore this dose was used in the following experiment.

G-CSF Promotes Re-Endothelialization

To evaluate re-endothelialization, Evans Blue dye was administered premortem to stain-remaining nonendothelialized areas. Re-endothelialized areas appear white (Figure 2A) and were significantly larger in G-CSF–treated rats than in the vehicle-injected group (63.0±6.8% versus 35.7±6.6%; n=10; $P<0.01$). Immunostaining revealed that the ratio of FactorVIII+ endothelial layer relative to the total luminal surface was significantly greater in G-CSF–treated rats than in the control (67.4±7.9% versus 40.2±6.9%; n=10; $P<0.01$; Figure 2B), indicating that G-CSF promoted re-endothelialization, leading to the inhibition of neointimal hyperplasia.

Functional Analysis of Regenerated Endothelium

NO production in the regenerated endothelium was measured by acetylcholine (Ach)-mediated relaxation of carotid artery preconstricted by norepinephrine. Ach caused a relaxation response in the normal carotid artery (30.9±1.8%, n=6) versus papaverine-induced maximal relaxation in an NO-dependent manner (as shown by N^G-nitro-L-arginine methyl ester [L-NAME] inhibition), whereas in the EC-injured artery, this response was markedly abolished (2.8±0.9%, n=6). In contrast, in the G-CSF–treated injured artery, relaxation was restored to a level comparable to that of normal carotid artery (43.8±4.5%; n=6), whereas L-NAME pretreatment completely inhibited such an Ach-mediated response (Figure 3), suggesting that the regenerated endothelium exerts an NO-mediated vasorelaxation response.

Endothelial Regeneration by G-CSF–Mobilized CEPCs

Because G-CSF was reported to increase CEPCs,[10,17] we next examined whether the G-CSF–mobilized CEPCs actually contributed to endothelial regeneration after EC-denuded injury. PB-MNCs (1×10^7 cells) were prepared from 5-day

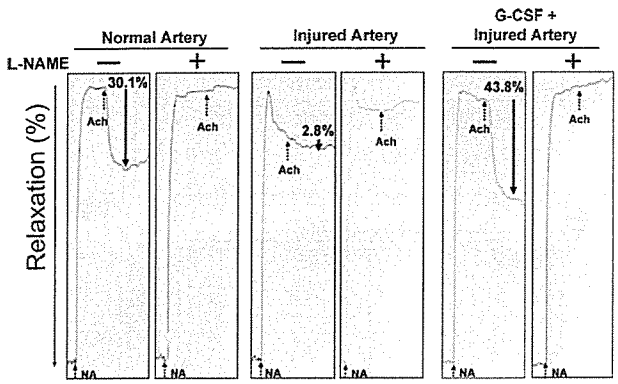

Figure 3. Ach-mediated relaxation of the carotid artery. Ach (10 μmol/L)-induced relaxation was examined using the carotid artery preconstricted with norepinephrine (30 nmol/L). The relaxation response was evaluated as a value relative to the papaverine-induced maximal relaxation (%) with or without L-NAME. Broken arrows show the time points to indicate drug administration. Solid arrows indicate Ach-induced vasorelaxation. Experiments were repeated 3 times with reproducible results. Representative data are shown.

G-CSF–treated or vehicle-injected donor rats, DiI-labeled, and transfused into the recipient rats after vascular injury. In the day-14 samples, DiI+ cells were incorporated into the neo-endothelium and double immunofluorescence with anti-CD31 antibody disclosed that DiI+ PB-MNCs derived from G-CSF–treated donor rats contributed to neoendothelium formation greater than the vehicle-injected rats (DiI+/CD31+ area 54.3±6.1% versus 6.3±1.2% to total luminal surface length; n=5; $P<0.01$; Figure 4A).

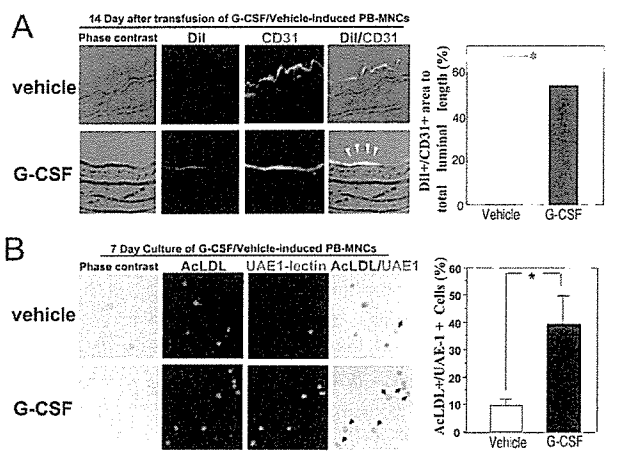

Figure 4. G-CSF increased the number of CEPCs. A, PB-MNCs were isolated from 5-day G-CSF–treated donor rats and labeled with DiI and transfused to the recipient rat after arterial injury (1×10^7 cells). On day 14, the injured lesion was removed, frozen-sectioned, and immunostained with FITC-conjugated anti-CD31 antibody. Localization of CD31+/DiI+ cells is indicated as yellow fluorescence in the merged image (arrowheads). Statistics: DiI+/CD31+ double fluorescent area in G-CSF–treated rat is greater than the vehicle-injected rat. *$P<0.05$ vs vehicle-treated group (n=6). B, PB-MNCs were cultured on fibronectin-coated plates for 7 days. EPC was identified with its binding ability to FITC–UAE-1-lectin and incorporation of DiI-AcLDL. Localization of UAE-1+/AcLDL+ cells is indicated by arrowheads in the merged image. Statistics: Percentage of double fluorescent cells relative to total adherent cells is presented (n=5; *$P<0.05$).

PB-MNCs from G-CSF–treated or vehicle-injected rats were primarily cultured for 7 days. EPC-like cells were identified by their binding ability to FITC–UEA1-lectin and uptake of DiI–AcLDL. The ratio of UAE-1+/AcLDL+ cells to total adherent cells from G-CSF–treated rats was 4-fold higher than that from vehicle-injected rats (39.2±9.8% versus 9.5±5.0% to total cultured cells; n=6; $P<0.05$; Figure 4B).

Endothelial Regeneration by G-CSF–Mobilized c-Kit+/Flk-1+ Cells

We studied the cell type responsible for endothelial regeneration induced by G-CSF. Because the anti-rat Flk-1 antibody for FACS sorting was not available, we analyzed the PB from "mice." Hematopoietic lineage negative (Lin-)/c-Kit+ cells were sorted from the mice PB and further analyzed for the expression of endothelial lineage markers Flk-1 and CD34. G-CSF treatment markedly elevated the ratio of Lin-/c-Kit+ cells to total PB-MNCs (8.1±0.5-fold; n=5; $P<0.01$), whereas the CD34+/Flk-1+ population included in the Lin-/c-Kit+ cells was increased 9.8±0.8-fold (n=5; $P<0.01$; Figure 5A).

To further elucidate the contribution of circulating c-Kit+/Flk-1+ cells to endothelial regeneration, 5×10^4 c-Kit+/Flk-1+/GFP+ or 1×10^6 c-Kit+/Flk-1-/GFP+ cells were isolated from enhanced GFP (EGFP) transgenic mice and injected into the nude rats after balloon injury. GFP mRNA transcription in the transgenic mice is driven by the chicken β-actin promoter and cytomegalovirus enhancer, indicating that the transcript expression in the hematopoietic and EC lineages is strong enough to trace them in the recipient mouse organ. In fact, GFP-positive ECs can be detected with a strong signal in the neo-endothelium. Figure 5B shows that GFP+ cells in the day-14 samples were detected on the regenerated endothelium of c-Kit+/Flk-1+ cell–transfused nude rats, and that these GFP+ cells were positive for the EC marker CD31 (Figure 5B, top, arrowheads), whereas the GFP+ cells were barely detectable in c-Kit+/Flk-1− cell–transfused nude rats (Figure 5B, bottom), suggesting that c-Kit+/Flk-1+ cells contain the cell population that can differentiate into CD31+ EC-like cells in the EC-denuded lesion.

Analysis by BM Replacement Model

To examine whether G-CSF–mobilized EPCs were originated from the BM, BM cells from EGFP transgenic mice were transplanted into the nude rats of which marrow cells had been ablated with whole body irradiation. Six weeks after transplantation, 86±2% of PB-MNCs were replaced (FACS; data not shown). The nude rats that received arterial injury and mobilization of BM-derived GFP+ cells to the neo-endothelium was examined on day 14. GFP+ cells were detected in the endothelial layer, and the immunostaining disclosed that CD31+/GFP+ EC-like cells were detected only in the G-CSF–treated group but not in the vehicle-injected group (39.2±5.8% versus 2.2±1.5% to total luminal surface length; n=5 each; $P<0.005$; Figure 6), indicating that 37.0% of the total luminal area (39.2% G-CSF group)−(2.2% saline group) was derived from G-CSF–mobilized BM cells (GFP+/CD31+ area). Considering that G-CSF–promoted neo-endothelium was 37.2% of the total luminal area (67.4%

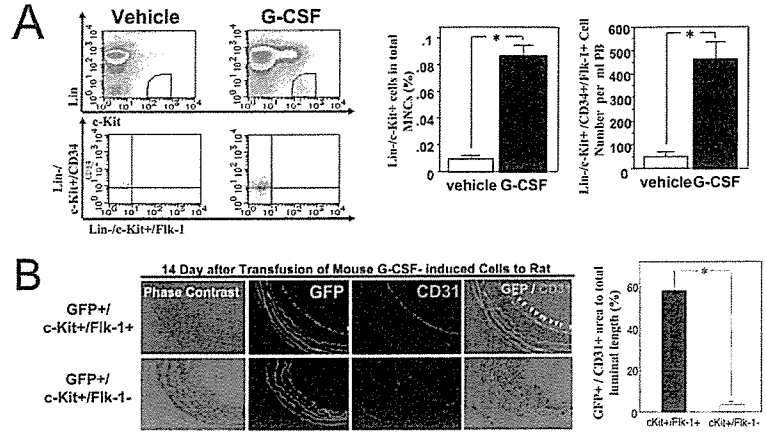

Figure 5. G-CSF–induced circulating c-Kit+/Flk-1+ cells differentiate to EC-like cells in the neo-endothelium. A, Five days after the injection of G-CSF, PB-MNCs were isolated, incubated with monoclonal antibodies (CD3-FITC, B220-FITC, CD11b-FITC, Gr1-FITC, NK1.1-FITC, Ter119-FITC, VEGFR-2-PE, and c-Kit-PE-Cy5) or with CD34-biotin, followed by activated protein C–avidine conjugated secondary antibody, and subjected to FACS analysis. The Lin-/c-Kit+ cell population was once gated (top left column) and subsequently analyzed for the expression of CD34 and Flk-1 (bottom left column). Statistical analysis: Percentage of Lin-/c-Kit+ cells to total MNCs or the absolute number of Lin-/c-Kit+/CD34+/Flk-1+ (right 2 panels) is significantly higher in G-CSF–treated group (n=5; *$P<0.01$ vs vehicle-injected group). B, Five days after the injection of G-CSF to GFP-overexpressing mice, PB-MNCs were collected, and 5×10^4 GFP+/c-Kit+/Flk-1+ or 1×10^6 GFP+/c-Kit+/Flk-1− cells were sorted and transfused to the nude rats after balloon injury. The lesion was removed on day 14, frozen sectioned, and subjected to immunostaining with rhodamine-conjugated antibody against CD31. CD31+/GFP+ cells appeared yellow in the merged image (arrowheads). *$P<0.01$ vs vehicle-treated group (n=5).

G-CSF group)−(40.2% saline group), these findings suggest that BM-derived cells are mainly involved in G-CSF–promoted neoendothelial formation, and the contribution of the G-CSF–mediated outgrowth of resident ECs is negligible.

Discussion

Because the natural regenerative process after EC-denuded injury is slow, it cannot prevent the onset of the neointimal lesions.[1] A novel approach that promotes re-endothelialization is required to accelerate this process. Several reports have shown that EPCs can be harvested from PB, and the intravenous injection of EPCs into EC-denuded vessels accelerates the recovery of endothelial integrity, resulting in the inhibition of neointimal hyperplasia and the restoration of vasodilatation activity.[4–7] The EPCs were shown to enhance the endothelialization of small-caliber prosthetic grafts.[14,15] G-CSF treatment increases the circulating CD34+ cells expressing endothelial markers,[10] and administration of G-CSF to patients with coronary artery disease increased the circulating MNCs with EPC properties.[23] Furthermore, G-CSF inhibited the neointimal formation in balloon-injured vessels,[17] whereas it remains undetermined what cell types of marrow-derived cells are directly involved in G-CSF–mediated endothelial regeneration. Furthermore, neither the functional properties of the regenerated endothelium were studied nor analysis using BM transplant experiments undertaken in G-CSF–treated animals. Our present study performed BM replacement experiments and clearly showed that G-CSF treatment increases the number of BM-derived c-Kit+/Flk-1+ EPCs that actually contribute to re-endothelialization of the balloon-injured arteries, leading to marked inhibition of neointimal formation. Furthermore, we found that the regenerated endothelium exerts Ach-mediated vasodilatory action in an NO-dependent manner. Interestingly, the injured arteries of G-CSF–treated rats have a better vasodilatory capacity compared with normal arteries. The data were analyzed in the 6 different animals with the reproducibility. Although we cannot sufficiently explain the molecular mechanism responsible for the better vasodilatory capacity, the neo-endothelium regenerated by G-CSF–mobilized BM cells or G-CSF–mediated direct action to the endothelial regeneration process might have the enhanced NO-mediated vasodilatory effect. Further studies will be required to clarify the underlying

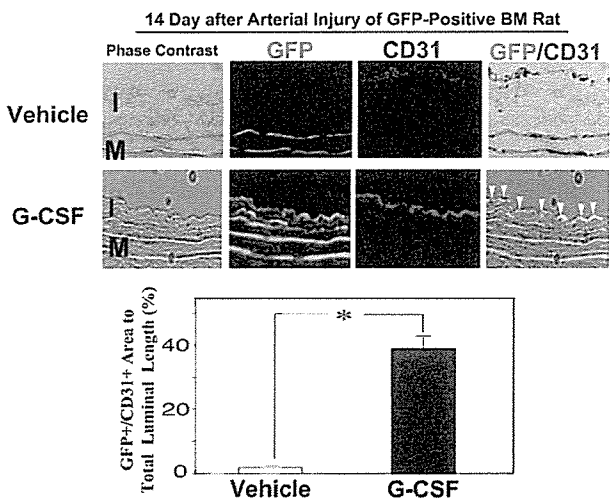

Figure 6. G-CSF–induced regenerated endothelium was originated from BM. Donor BM from EGFP-overexpressing mice was transfused to the BM-ablated nude rats. Recipient rats were balloon injured, and G-CSF or vehicle was injected daily for 14 days from 3 days before arterial injury. On day 14, the lesions were removed and immunostained with rhodamine-conjugated anti-CD31 antibody. CD31+/GFP+ cells appeared yellow in the merged image (arrowheads). Double fluorescent cells were detected on the neoendothelium in the G-CSF–treated nude rats (bottom panels), whereas they were barely detectable in the vehicle-treated nude rats (top panels). *$P<0.005$ vs vehicle-treated group (n=5).

mechanism. Together, this evidence leads us to consider a more aggressive clinical use of G-CSF to mobilize CEPCs and promote vascular repair.

It appears that the safety and feasibility of G-CSF treatment focusing on the induction of vascular occlusion in atherosclerotic lesions has not yet been established.[24] In angina patients, the administration of G-CSF was associated with the onset of acute myocardial infarction (AMI).[25] A high rate of restenosis after intracoronary infusion of G-CSF–mobilized PB-MNCs was reported in AMI patients.[16] There are articles reporting the induction of AMI and cerebral infarction in G-CSF–treated BM transplantation patients.[26,27] Differentiation of G-CSF–mobilized progenitor cells into smooth muscle cells within the stented segment as well as the induction of angiogenesis within the atherosclerotic lesion and the aggregation of mobilized inflammatory cells within the plaque may be a plausible explanation.[24] Furthermore, G-SCF–mobilized neutrophils may cause EC damage by superoxide production.[28–30] We have previously shown that polymorphonuclear cells inhibited the ischemia-induced recovery of blood perfusion in the hindlimb ischemia model.[31] Furthermore, G-CSF induces the expression of adhesion molecules on ECs, leading to leukocyte adhesion and its activation[32] or to a hypercoagulability state.[33] Thus, because G-CSF induces non-EPC populations, including neutrophil or smooth muscle progenitor cells, the enrichment of the EPC population and their application are required to inhibit such harmful effects. Indeed, the injection of G-CSF–induced circulating CD34+EPCs into ischemic limb muscle resulted in satisfactory clinical improvement.[34] Transplantation of an enriched CD34+MNC population re-established endothelial integrity in injured vessels, thereby inhibiting neointimal hyperplasia.[4] We here described that a small number (5×10^4) of enriched population c-Kit+/Flk-1+ or CD45-/Flk-1+ EPCs regenerated endothelium much more efficiently than did a large number (1×10^6) of c-Kit+/Flk-1− or CD45-/Flk-1− cells. Consistent with our observation, in the hindlimb ischemia model of mice, merely 1×10^3 CD34+/Flk-1+ cells improved limb salvage and hemodynamic recovery better than 1×10^4 CD34+/Flk-1− cells.[35] Thus, the application of an enriched EPC population may be feasible to improve the safety and efficiency of G-CSF therapy.

Increasing evidence suggests that BM-derived EPCs home to the ischemic region for the formation of new blood vessels.[2] EPCs were reportedly derived from more differentiated CD34+ or immature CD133+ hematopoietic stem cells, as well as from mature PB-MNCs or CD14+ monocytes.[5,36] They express endothelial markers, including Flk-1, FactorVIII, and endothelial NO synthase.[2,36] Intravenous infusion of BM-derived EPCs enhanced neovascularization in vivo.[37] Application of either BM-derived or PB-derived EPCs into the infarct artery beneficially affects postinfarction remodeling.[38,39] Consistent with these previous reports, we presented the data indicating that the c-Kit+/Flk-1+ cells were actually mobilized by G-CSF administration (Figure 5A), and the infusion experiment of the sorted c-Kit+/Flk-1+ EGFP cells (mobilized by G-CSF) revealed their direct involvement in the G-CSF–promoted endothelial regeneration process in the vascular repair. Thus, the stem cells expressing the Flk-1 marker are mobilized in response to G-CSF and then exert the property as an endothelial progenitor, suggesting that c-Kit+/Flk-1+ cells are the cell type responsible for G-CSF–mediated endothelial regeneration.

In conclusion, we characterized the cell type responsible for G-CSF–mediated endothelial regeneration leading to an inhibition of neointimal hyperplasia and showed that the vascular repair was mainly attributable to the G-CSF–mobilized BM-derived cells rather than G-CSF–mediated outgrowth of resident ECs, and that the repaired artery responded well to NO-mediated vasodilatory stimulus. These findings suggest that the treatment with G-CSF might be a feasible and suitable supplement therapy for the prevention of restenosis after the revascularization procedures. Although the very recent clinical study has reported that administration of G-CSF to patients with AMI improves cardiac function without any adverse events during 6-month observation,[40] G-CSF–mediated proatherogenic effects, such as the induction of angiogenesis within the atherosclerotic lesion and the aggregation of mobilized inflammatory cells within the atheromatous plaque, are the limitation of the present study and remain to be determined. Further basic and clinical studies focusing on these issues will be required.

Acknowledgments

This work was supported in part by a grant from the Ministry of Education, Culture, Science and Technology of Japan. We appreciate Dr Takeshi Todo for his great help in BM replacement experiment.

References

1. Libby P, Schwartz D, Brogi E, Tanaka H, Clinton SK. A cascade model for restenosis. A special case of atherosclerosis progression. *Circulation.* 1992;86:III47–III52.
2. Asahara T, Murohara T, Sullivan A, Silver M, van der Zee R, Li T, Witzenbichler B, Schatteman G, Isner JM. Isolation of putative progenitor endothelial cells for angiogenesis. *Science.* 1997;275:964–967.
3. Asahara T, Masuda H, Takahashi T, Kalka C, Pastore C, Silver M, Kearne M, Magner M, Isner JM. Bone marrow origin of endothelial progenitor cells responsible for postnatal vasculogenesis in physiological and pathological neovascularization. *Circ Res.* 1999;85:221–228.
4. Griese DP, Ehsan A, Melo LG, Kong D, Zhang L, Mann MJ, Pratt RE, Mulligan RC, Dzau VJ. Isolation and transplantation of autologous circulating endothelial cells into denuded vessels and prosthetic grafts: implications for cell-based vascular therapy. *Circulation.* 2003;108:2710–2715.
5. Fujiyama S, Amano K, Uchira K, Yoshida M, Nishiwaki Y, Nozawa Y, Jin D, Takai S, Miyazaki M, Egashira K, Imada T, Iwasaka T, Matsubara H. Bone marrow monocyte lineage cells adhere on injured endothelium in a monocyte chemoattractant protein-1-dependent manner and accelerate reendothelialization as endothelial progenitor cells. *Circ Res.* 2003;93:980–989.
6. Werner N, Junk S, Laufs U, Link A, Walenta K, Bohm M, Nickenig G. Intravenous transfusion of endothelial progenitor cells reduces neointima formation after vascular injury. *Circ Res.* 2003;93:e17–24.
7. Gulati R, Jevremovic D, Peterson TE, Witt TA, Kleppe LS, Mueske CS, Lerman A, Vile RG, Simari RD. Autologous culture-modified mononuclear cells confer vascular protection after arterial injury. *Circulation.* 2003;108:1520–1526.
8. Lapidot T, Petit I. Current understanding of stem cell mobilization: the roles of chemokines, proteolytic enzymes, adhesion molecules, cytokines, and stromal cells. *Exp Hematol.* 2002;30:973–981
9. Takahashi T, Kalka C, Masuda H, Chen D, Silver M, Kearney M, Magner M, Isner JM, Asahara T. Ischemia- and cytokine-induced mobilization of bone marrow-derived endothelial progenitor cells for neovascularization. *Nat Med.* 1999;5:434–438.
10. Kocher AA, Schuster MD, Szabolcs MJ, Takuma S, Burkhoff D, Wang J, Homma S, Edwards NM, Itescu S. Neovascularization of ischemic

myocardium by human bone-marrow-derived angioblasts prevents cardiomyocyte apoptosis, reduces remodeling and improves cardiac function. *Nat Med.* 2001;7:430–436.
11. Shyu WC, Lin SZ, Yang HI, Tzeng YS, Pang CY, Yen PS, Li H. Functional recovery of stroke rats induced by granulocyte colony-stimulating factor-stimulated stem cells. *Circulation.* 2004;110: 1847–1854.
12. Cotter M, Gulmann C, Jeffers M, Smith OP. Increased bone marrow angiogenesis in children with severe chronic neutropenia treated with granulocyte colony-stimulating factor. *J Pediatr Hematol Oncol.* 2004; 26:504–506.
13. Minamino K, Adachi Y, Okigaki M, Ito H, Togawa Y, Fujita K, Tomita M, Suzuki Y, Zhang Y, Iwasaki M, Nakano K, Koike Y, Matsubara H, Iwasaka T, Matsumura M, Ikehara S. Macrophage colony-stimulating factor (M-CSF), as well as granulocyte colony-stimulating factor (G-CSF), accelerates neovascularization. *Stem Cells.* 2005;23:347–354.
14. Bhattacharya V, Shi Q, Ishida A, Sauvage LR, Hammond WP, Wu MH. Administration of granulocyte colony-stimulating factor enhances endothelialization and microvessel formation in small caliber synthetic vascular grafts. *J Vasc Surg.* 2000;32:116–123.
15. Shi Q, Bhattacharya V, Hong-De Wu M, Sauvage LR. Utilizing granulocyte colony-stimulating factor to enhance vascular graft endothelialization from circulating blood cells. *Ann Vasc Surg.* 2002;16:314–320.
16. Kang HJ, Kim HS, Zhang SY, Park KW, Cho HJ, Koo BK, Kim YJ, Soo Lee D, Sohn DW, Han KS, Oh BH, Lee MM, Park YB. Effects of intracoronary infusion of peripheral blood stem-cells mobilised with granulocyte-colony stimulating factor on left ventricular systolic function and restenosis after coronary stenting in myocardial infarction: the MAGIC cell randomised clinical trial. *Lancet.* 2004;363:751–756.
17. Kong D, Melo LG, Mangi AA, Zhang L, Lopez-Ilasaca M, Perrella MA, Liew CC, Pratt RE, Dzau VJ. Cytokine-induced mobilization of circulating endothelial progenitor cells enhances repair of injured arteries. *Circulation.* 2004;110:2039–2046.
18. Okabe M, Ikawa M, Kominami K, Nakanishi T, Nishimune Y. 'Green mice' as a source of ubiquitous green cells. *FEBS Lett.* 1997;407: 313–319.
19. Minatoguchi S, Takemura G, Chen XH, Wang N, Uno Y, Koda M, Arai M, Misao Y, Lu C, Suzuki K, Goto K, Komada A, Takahashi T, Kosai K, Fujiwara T, Fujiwara H. Acceleration of the healing process and myocardial regeneration may be important as a mechanism of improvement of cardiac function and remodeling by postinfarction granulocyte colony–stimulating factor treatment. *Circulation.* 2004;109:2572–2580.
20. Chen X, Kelemen SE, Autieri MV. Expression of granulocyte colony-stimulating factor is induced in injured rat carotid arteries and mediates vascular smooth muscle cell migration. *Am J Physiol Cell Physiol.* 2005; 288:C81–C88.
21. Bussolino F, Ziche M, Wang JM, Alessi D, Morbidelli L, Cremona O, Bosia A, Marchisio PC, Mantovani A. In vitro and in vivo activation of endothelial cells by colony-stimulating factors. *J Clin Invest.* 1991;87: 986–995.
22. Sudo Y, Shimazaki C, Ashihara E, Kikuta T, Hirai H, Sumikuma T, Yamagata N, Goto H, Inaba T, Fujita N, Nakagawa M. Synergistic effect of FLT-3 ligand on the granulocyte colony-stimulating factor-induced mobilization of hematopoietic stem cells and progenitor cells into blood in mice. *Blood.* 1997;89:3186–3191.
23. Powell TM, Paul JD, Hill JM, Thompson M, Benjamin M, Rodrigo M, McCoy JP, Read EJ, Khuu HM, Leitman SF, Finkel T, Cannon RO III. Granulocyte colony-stimulating factor mobilizes functional endothelial progenitor cells in patients with coronary artery disease. *Arterioscler Thromb Vasc Biol.* 2005;25: 296–301.
24. Matsuabara H. Risk to the coronary arteries of intracoronary stem cell infusion and G-CSF cytokine therapy. *Lancet.* 2004;363:746–747.
25. Hill JM, Syed MA, Arai AE, Powell TM, Paul JD, Zalos G, Read EJ, Khuu HM, Leitman SF, Horne M, Csako G, Dunbar CE, Waclawiw MA, Cannon RO III. Outcomes and risks of granulocyte colony-stimulating factor in patients with coronary artery disease. *J Am Coll Cardiol.* 2005;46: 1643–8.
26. Kawachi Y, Watanabe A, Uchida T, Yoshizawa K, Kurooka N, Setsu K. Acute arterial thrombosis due to platelet aggregation in a patient receiving granulocyte colony-stimulating factor. *Br J Haematol.* 1996;94:413–416.
27. Fukumoto Y, Miyamoto T, Okamura T, Gondo H, Iwasaki H, Horiuchi T, Yoshizawa S, Inaba S, Harada M, Niho Y. Angina pectoris occuring during granulocyte colony-stimulating factor-combined preparatory regimen for autologous peripheral blood stem cell transplantation in a patient with acute myelogenous leukemia. *Br J Haematol.* 1997;97: 666–668.
28. Hierholzer C, Kelly E, Lyons V, Roedling E, Davies P, Billiar TR, Tweardy DJ. G-CSF instillation into rat lungs mediates neutrophil recruitment, pulmonary edema, and hypoxia. *J Leukoc Biol.* 1998;63: 169–174.
29. Azoulay E, Attalah H, Yang K, Jouault H, Schlemmer B, Brun-Buisson C, Brochard L, Harf A, Delclaux C. Exacerbation by granulocyte colony-stimulating factor of prior acute lung injury: implication of neutrophils. *Crit Care Med.* 2002;30:2115–2122.
30. Hardy MM, Flickinger AG, Riley DP, Weiss RH, Ryan US. Superoxide dismutase mimetics inhibit neutrophil-mediated human aortic endothelial cell injury in vitro. *J Biol Chem.* 1994;269:18535–18540.
31. Iba O, Matsubara H, Nozawa Y, Fujiyama S, Amano K, Mori Y, Kojima H, Iwasaka T. Angiogenesis by implantation of peripheral blood mononuclear cells and platelets into ischemic limbs. *Circulation.* 2002;8;106: 2019–2025.
32. Fuste B, Mazzara R, Escolar G, Merino A, Ordinas A, Diaz-Ricart M. Granulocyte colony-stimulating factor increases expression of adhesion receptors on endothelial cells through activation of p38 MAPK. *Haematologica.* 2004;89:578–585.
33. Canales MA, Arrieta R, Gomez-Rioja R, Diez J, Jimenez-Yuste V, Hernandez-Navarro F. Induction of a hypercoagulability state and endothelial cell activation by granulocyte colony-stimulating factor in peripheral blood stem cell donors. *J Hematother Stem Cell Res.* 2002;11: 675–681.
34. Kudo FA, Nishibe T, Nishibe M, Yasuda K. Autologous transplantation of peripheral blood endothelial progenitor cells (CD34+) for therapeutic angiogenesis in patients with critical limb ischemia. *Int Angiol.* 2003;22: 344–348.
35. Madeddu P, Emanueli C, Pelosi E, Salis MB, Cerio AM, Bonanno G, Patti M, Stassi G, Condorelli G, Peschle C. Transplantation of low dose CD34+KDR+ cells promotes vascular and muscular regeneration in ischemic limbs. *FASEB J.* 2004;18:1737–1739.
36. Urbich C, Dimmeler S. Endothelial progenitor cells: characterization and role in vascular biology. *Circ Res.* 2004;95:343–353.
37. Shintani S, Murohara T, Ikeda H, Ueno T, Sasaki K, Duan J, Imaizumi T. Augmentation of postnatal neovascularization with autologous bone marrow transplantation. *Circulation.* 2001;103:897–903.
38. Strauer BE, Brehm M, Zeus T, Kostering M, Hernandez A, Sorg RV, Kogler G, Wernet P. Repair of infarcted myocardium by autologous intracoronary mononuclear bone marrow cell transplantation in humans. *Circulation.* 2002;106:1913–1918.
39. Assmus B, Schachinger V, Teupe C, Britten M, Lehmann R, Dobert N, Grunwald F, Aicher A, Urbich C, Martin H, Hoelzer D, Dimmeler S, Zeiher AM Transplantation of Progenitor Cells and Regeneration Enhancement in Acute Myocardial Infarction (TOPCARE-AMI). *Circulation.* 2002;106:3009–3017.
40. Valgimigli M, Rigolin GM, Cittanti C, Malagutti P, Curello S, Castoldi G, Ferrari R. Use of granulocyte-colony stimulating factor during acute myocardial infarction to enhance bone marrow stem cell mobilization in humans: clinical and angiographic safety profile. *Eur Heart J.* 2005;26: 1838–1845.

Arteriosclerosis, Thrombosis, and Vascular Biology

JOURNAL OF THE AMERICAN HEART ASSOCIATION

Targeted Delivery of Bone Marrow Mononuclear Cells by Ultrasound Destruction of Microbubbles Induces Both Angiogenesis and Arteriogenesis Response

Takanobu Imada, Tetsuya Tatsumi, Yasukiyo Mori, Takashi Nishiue, Masayuki Yoshida, Hiroya Masaki, Mitsuhiko Okigaki, Hiroyuki Kojima, Yoshihisa Nozawa, Yasunobu Nishiwaki, Noriko Nitta, Toshiji Iwasaka and Hiroaki Matsubara

Arterioscler. Thromb. Vasc. Biol. 2005;25;2128-2134; originally published online Jul 28, 2005;
DOI: 10.1161/01.ATV.0000179768.06206.cb
Arteriosclerosis, Thrombosis, and Vascular Biology is published by the American Heart Association. 7272 Greenville Avenue, Dallas, TX 72514
 Print ISSN: 1079-5642. Online ISSN: 1524-4636

Targeted Delivery of Bone Marrow Mononuclear Cells by Ultrasound Destruction of Microbubbles Induces Both Angiogenesis and Arteriogenesis Response

Takanobu Imada, Tetsuya Tatsumi, Yasukiyo Mori, Takashi Nishiue, Masayuki Yoshida, Hiroya Masaki, Mitsuhiko Okigaki, Hiroyuki Kojima, Yoshihisa Nozawa, Yasunobu Nishiwaki, Noriko Nitta, Toshiji Iwasaka, Hiroaki Matsubara

Objective—Ultrasound (US)-mediated destruction of contrast microbubbles causes capillary rupturing that stimulates arteriogenesis, whereas intramuscular implantation (im) of bone marrow mononuclear cells (BM-MNCs) induces angiogenesis. We therefore studied whether US-targeted microbubble destruction combined with transplantation of BM-MNCs can enhance blood flow restoration by stimulating both angiogenesis and arteriogenesis.

Methods and Results—US-mediated destruction of phospholipid-coated microbubbles was applied onto ischemic hindlimb muscle and subsequently BM-MNCs were transfused. A significant enhancement in blood flow recovery after Bubble+US+BM-MNC infusion (34% increase, $P<0.05$) was observed compared with Bubble+US (25%). The ratio of capillary/muscle fiber increased by Bubble+US+BM-MNC-i.v (260%, $P<0.01$) than that in the Bubble+US group (172%), into which BM-MNCs were incorporated (angiogenesis). Smooth muscle α-actin–positive arterioles were also increased, and angiography showed augmented collateral vessel formation (arteriogenesis). Platelet-derived proinflammatory factors activated by Bubble+US induces the expression of adhesion molecules (P-selectin and ICAM-1), leading to the attachment of transplanted BM-MNCs on the endothelium. Flow assay confirmed that the platelet-derived factors cause the adhesion of BM-MNCs onto endothelium under laminar flow.

Conclusions—This study demonstrates that the targeted delivery of BM-MNCs by US destruction of microbubbles enhances regional angiogenesis and arteriogenesis response, in which the release of platelet-derived proinflammatory factors activated by Bubble+US play a key role in the attachment of transplanted BM-MNCs onto the endothelial layer. (***Arterioscler Thromb Vasc Biol.* 2005;25:2128-2134.**)

Key Words: angiogenesis ■ vasculogenesis ■ stem cell ■ endothelial progenitor cell ■ ultrasound

Therapeutic angiogenesis, the ability to induce the formation of new blood vessels, is one of the most promising targets for regeneration therapy. To induce angiogenesis, investigators have delivered vascular endothelial growth factor (VEGF), basic fibroblast growth factor (bFGF/FGF2). or hypoxia-inducible factor-1α/etoposide as recombinant proteins or genes.[1] Intramuscular injection of bone marrow mononuclear cells (BM-MNCs) was shown to be feasible in patients or animals with ischemic limbs by supplying angiogenic factors and endothelial progenitors.[2–4] A noninvasive cell delivery system that can target vascular endothelium would be a great advantage for manipulation of angiogenic cell therapy.

Ultrasound (US)-targeted microbubble destruction has been investigated as a new method for delivering drugs and genes to specific tissues.[5–11] This method involves the attachment of drugs or genes to gas-filled microbubbles, which are then circulated through the intravascular space and mechanically destroyed within the target organ. Theoretically, one can target any anatomic site that is accessible by US, including selected damaged regions.[5–11] Song et al have reported that US-targeted microbubble destruction causes capillary rupturing that stimulates arteriogenesis and an increase in blood flow in both normal[12] and ischemic[13] skeletal muscles, in which angiogenesis response is transient and unlikely contributes to chronic restoration of blood flow. We previously demonstrated that the recruitment of BM-MNCs and platelets stimulates angiogenesis response in ischemic muscles by releasing potent angiogenic factors, such as VEGF or bFGF, and supply of endothelial progenitors.[3,14] Furthermore, we have recently reported that systemically

Original received December 27, 2004; final version accepted May 18, 2005.

From the Department of Medicine II (T. Imada, Y.M., T.N., H. Masaki, T. Iwasaka) and Radiology (H.K.), Kansai Medical University, Osaka; the Department of Cardiovascular Medicine (T.T., M.O., H. Matsubara), Kyoto Prefectural University School of Medicine, Kyoto; the Department of Medical Biochemistry (M.Y., Y. Nishiwaki, N.N.), Graduate School of Medicine, Tokyo Medical and Dental University, Tokyo; and the Pharmacobioregulation Research Laboratory (Y. Nozawa), Taiho Pharmaceutical Co Ltd, Saitama, Japan.

T. Iwasaka and H. Matsubara contributed equally to this study.

Correspondence to Hiroaki Matsubara MD, Department of Cardiovascular Medicine, Kyoto Prefectural University School of Medicine, Kamigyo-ku, Kyoto, 602-8566, Japan. E-mail matsubah@koto.kpu-m.ac.jp

Arterioscler Thromb Vasc Biol. **is available at http://www.atvbaha.org** **DOI: 10.1161/01.ATV.0000179768.06206.cb**

transplanted BM-MNCs can be firmly attached onto the injured vascular endothelium in an adhesive molecule–dependent manner.[15] We therefore examined whether US-targeted microbubble destruction combined with intravenous transplantation of BM-MNCs causes angiogenesis response as well as arteriogenesis in a rat model with an ischemic hindlimb, leading to an enhancement of chronic blood flow restoration. Interestingly, we found that platelet-derived factors activated by US-targeted microbubble destruction induce the expression of adhesive molecules on the endothelium and subsequent attachment of transplanted BM-MNCs, resulting in an enhancement of formation of neocapillaries and new arterioles and an increase in regional blood flow recovery.

Materials and Methods

Microbubble Preparations

BR14 (Bracco Diagnostics) is a new ultrasound contrast agent, consisting of perfluorocarbon-containing microbubbles stabilized by a phospholipid monolayer.[16,17] The suspension of gas microbubbles is reconstituted immediately before use by injecting 5 mL of 0.9% sodium chloride. The mean diameter of bubbles is 2.3 to 2.5 μm and the bubble concentration is $\approx 6\times10^8$ per ml. BR14 was administered as a 1 mL bolus injection via contralateral femoral vein.

Isolation of BM-MNC and Characterization of Endothelial-Lineage Cells

BM-MNCs were isolated from SEA/LEW rat femoral bone and centrifuged by density gradient (Lymphoprep; Nycomed). The MNC fraction was labeled with red-fluorescence cell linker (PKH26-GL; Sigma).[2,3,14] Endothelial lineage cells were analyzed by fluorescence-activated cell sorter (FACS) using DiI-acetylated LDL (acLDL) incorporation (Biogenesis) and Ulex lectin binding (Sigma) as described previously.[2,3,14]

Hindlimb Ischemia, US Application, and Transfusion of BM-MNCs

Unilateral hindlimb ischemia was induced by resecting the left femoral artery as described.[2,18] Arteriogenesis that restores the regional blood flow was reported to be observed 3 days after induction of limb ischemia of rats.[12,13] We therefore performed the infusion of microbubble at day 3 after limb ischemia to efficiently deliver microbubble BR14 to the ischemic site. We divided the rats into the following five groups: (1) Control (saline injection, n=8); (2) Bubble (1 mL BR14)+US (n=8); (3) Bubble+US+BM-MNC-i.v. (n=8), BM-MNC (2×10^7 in 1 mL saline) injected from contralateral femoral vein 1 minute after Bubble+US; (4) BM-MNC-i.m. (n=8), BM-MNC (2×10^7) intramuscularly implanted into the ischemic limb; and (5) BM-MNC-i.v. (n=8); BM-MNC (2×10^7 in 1 mL saline). BM-MNC (2×10^7) included $0.3\pm0.04\times10^7$ platelets.

The skin overlying the ischemic thigh muscle to be treated was reflected back, ultrasound gel was placed over the ischemic muscle, and 1-MHz transducer (S-probe, Effective Radiating Area: 0.9 cm^2; Ito Co Ltd) was held 3 mm over the muscle and to keep the skin temperature around $\approx$37°C. A continuous sinusoidal wave ultrasound (1MHz, 2W/cm^2, Beam Nonuniformity Ratio: 3.6; ITO-US-700) was applied for 1 minute immediately after microbubble injection. To clarify whether the microbubbles really reach ischemic tissues after infusion from contralateral femoral vein, the delivery of injected microbubbles to the ischemic area was examined by a diagnostic ultrasound echography (Sonos-5500) equipped with an ultraband S12 sector transducer.

Evaluation of Neocapillary and Immunohistochemical Analysis

Four pieces of ischemic tissues from the adductor and semimembranous muscles were obtained 28 days after limb ischemia. Frozen sections were stained with antibodies for smooth muscle (SM) α-actin (Sigma) and anti-factor VIII (DAKO) antibodies. The appropriate secondary antibodies conjugated with fluorescein isothiocyanate (FITC) or rhodamine were used. Ten fields from 2 muscle samples of each animal were randomly selected for the vessel count. To ensure that vessel densities were not overestimated as a consequence of myocyte atrophy or underestimated because of interstitial edema, the capillary/muscle fiber ratio was determined.[3,18]

Electron Microscope

Femoral arteries in skeletal muscles on which targeted US was applied were isolated after Bubble+US treatment (n=4), fixed by 2.5% glutaraldehyde and 1.5% osmium acid, dried, and viewed by electron microscope (HITATI S-700).[15]

Cell Culture and Platelet-Rich Plasma Isolation

Human umbilical vein endothelial cells (HUVECs; Kurabo) were cultured in HuMedia-EG2 medium. For use in the study apparatus, HUVECs (2nd or 3rd passages) were plated on 22-mm fibronectin-coated cover slips.[15] Peripheral blood was drawn from healthy volunteers and mixed with 0.1 volume of citrate (108 mmol/L). Whole blood was centrifuged at 150g for 10 minutes to harvest platelet-rich plasma (PRP).

Adhesion Assay Under Laminar Flow and Immunofluorescence Study

HUVECs were incubated for 30 minutes with serum-free medium with or without freshly prepared 10% platelet-rich plasma, and then stimulated by (1) 10% Bubble+US (1MHz, 1.5W, 30 seconds) in 10% PRP (Bubble+US with platelet group), (2) 10% Bubble+US in PRP (Bubble+US without platelet), (3) incubation media (in which 10% platelet-rich medium was stimulated by 10% Bubble+US), or (4) US with platelet (in which 10% platelet-rich medium was stimulated by US alone), n=6 in each experiment. HUVECs were placed on the cold plate to prevent the heating by the US, and adhesion assay under laminar flow was performed as previously described.[15] For further detail, please see the supplemental Methods, available online at http://atvb.ahajournals.org.

Stimulated HUVECs were fixed by 4% paraformaldehyde 1 hour after stimulation and incubated with anti–P-selectin (R&D Systems, Inc) and anti-platelet glycoprotein (GP)-Ib antibody (DAKO). The appropriate secondary antibodies conjugated with FITC or rhodamine were used. Nuclei were stained with 4′,6′-diamidino-2-phenylindole dihydrochloride (DAPI) and viewed by a fluorescence microscope (Olympus OX71).

Laser Doppler Perfusion Image and Angiography

Laser doppler perfusion image (LDPI) and angiography were performed as previously described[3,18] For further detail, please see the supplemental Methods.

Statistical Analysis

Statistical analyses were performed with 1-way ANOVA followed by pair-wise contrasts using the Dunnett test. Data (mean±SE) were considered statistically significant when $P<0.05$.

Results

Incidence of Endothelial-Lineage Cells in BM-MNCs

FACS analysis indicated that 28±1.8% and 31±1.5% of BM-MNCs incorporated DiI-acLDL and bound Ulex-lectin (n=5), respectively, and 20±1.2% of cells were positive for both markers. Endothelial-lineage cells were considered to be included in this fraction as reported.[2,3,14]